

# Plesio-Geostrophy and Data Assimilation: Products Results and Discussions

Jingtao Min

Feb 1, 2024, last update May 31, 2025

# Chapter 1

## Solutions to the eigenvalue problems

I present here the solutions to the eigenvalue problems in the PG model. The full PG model is a dynamical system described by system of PDEs

$$\mathcal{M}_i \frac{\partial x_i}{\partial t} = \mathcal{F}_i(x_1, \dots, x_N), \quad i = 1, 2, \dots, N.$$

$x_i$  are the dynamical variables in the PG model,  $\Psi$ ,  $\overline{M_{ss}}$ ,  $\overline{M_{\phi\phi}}$ , etc. If the boundary magnetic field is described by  $B_r$ , then  $N = 15$ ; alternatively, if the boundary magnetic field is described by  $B_s^\pm$ ,  $B_\phi^\pm$  and  $B_z^\pm$ , then  $N = 20$ . The former provides a closed system under certain boundary conditions, but requires a cylindrical-to-spherical transform. On the other hand, the latter is intrinsically in cylindrical coordinates, but is not closed in the nonlinear case. However, in eigenvalue problems with static background flow, the latter formulation is closed. For details, refer to the Ingredients document. Introducing

$$\mathcal{M} = \begin{pmatrix} \mathcal{M}_1 & & \\ & \ddots & \\ & & \mathcal{M}_N \end{pmatrix}, \quad \mathcal{F} = \begin{pmatrix} \mathcal{F}_1 \\ \vdots \\ \mathcal{F}_N \end{pmatrix}, \quad \mathbf{x} = \begin{pmatrix} x_1 \\ \vdots \\ x_N \end{pmatrix},$$

we can formally write the system as

$$\mathcal{M} \frac{\partial \mathbf{x}}{\partial t} = \mathcal{F}(\mathbf{x}).$$

If we consider perturbations near a time-invariant background field denoted as  $\mathbf{x}^0$ , the perturbed quantities follow the linearized equations

$$\mathcal{M} \frac{\partial \mathbf{x}}{\partial t} = D\mathcal{F}(\mathbf{x}^0) \mathbf{x} = \frac{\partial \mathcal{F}(\mathbf{x}^0)}{\partial \mathbf{x}^0} \mathbf{x} = \mathcal{K}(\mathbf{x}^0) \mathbf{x}.$$

This linear, autonomous dynamical system admits general solutions in the form of time-harmonic functions  $\mathbf{x}(t) = \mathbf{x}(0)e^{\lambda t} = \mathbf{x}^0 e^{i\tilde{\omega}t}$ . The purpose of this chapter is therefore to present the solution of eigenvalues  $\lambda$  and eigenmodes  $\mathbf{x}(t=0)$  to the eigenvalue problem in the form of

$$\lambda \mathcal{M} \mathbf{x} = i\tilde{\omega} \mathcal{M} \mathbf{x} = \mathcal{K}(\mathbf{x}^0) \mathbf{x}. \quad (1.1)$$

Unless otherwise specified, throughout this chapter the term *eigenvalue* refers to  $\lambda = i\tilde{\omega} \in \mathbb{C}$  defined in eq.(1.1).  $\sigma = \text{Re}[\lambda]$  gives the exponential growth / decay rate, while  $\omega = \text{Im}[\lambda]$  gives the angular frequency of temporal oscillations (*eigenfrequency*). For systems free of both viscous and magnetic diffusion, physics dictates that  $\text{Re}[\lambda] = 0$  or  $\tilde{\omega} = \omega$ , except for small numerical errors. Hereinafter such systems are described as *ideal*.

I shall present the solutions to the eigenvalue problems under several background fields  $\mathbf{x}^0$ . In each case, I shall provide the solved system, simplified equation, spectrum of the system, as well as selected eigenmodes. In this chapter, *the spectrum of a system or matrix* refers to the set of eigenvalues, whereas *the spectrum of an eigenmode* refers to the composition of the mode in terms of basis functions.

## 1.1 Inviscid hydrodynamic eigenmodes

We start by considering the eigenmodes in absence of magnetic fields in the inviscid limit. From the ideal PG equations, it means that the system is linearized around a background state where both the velocity and the magnetic fields are zero.

### 1.1.1 Linearized equations

The PG system in purely inviscid hydrodynamic case comprises only of the streamfunction equation,

$$\left[ \frac{\partial}{\partial s} \left( \frac{s}{H} \frac{\partial}{\partial s} \right) + \left( \frac{1}{sH} + \frac{s}{2H^3} \right) \frac{\partial^2}{\partial \phi^2} \right] \frac{\partial \psi}{\partial t} = \frac{2s}{H^3} \frac{\partial \psi}{\partial \phi} \quad (1.2)$$

while all magnetic quantities vanish. There is no difference between the PG equation, the transformed equation, or the reduced dimensional formulation, as only the streamfunction is relevant. Note for the hydrodynamic case, the rotation timescale  $\tau = \Omega^{-1}$  is used.

### 1.1.2 Standard ODE form

Using the Fourier ansatz  $\psi = \psi^m(s)e^{i\tilde{\omega}t+im\phi} = \psi^m(s)e^{\lambda t+im\phi}$ , the streamfunction equation can be written as an ODE in cylindrical radius  $s$ ,

$$\begin{aligned} \lambda \left[ \frac{d}{ds} \left( \frac{s}{H} \frac{d}{ds} \right) - m^2 \left( \frac{1}{sH} + \frac{s}{2H^3} \right) \right] \psi^m &= \frac{2s}{H^3} i m \psi^m \\ \tilde{\omega} \left[ \frac{d}{ds} \left( \frac{s}{H} \frac{d}{ds} \right) - m^2 \left( \frac{1}{sH} + \frac{s}{2H^3} \right) \right] \psi^m &= \frac{2s}{H^3} m \psi^m \\ \left[ \frac{d}{ds} \left( \frac{s}{H} \frac{d}{ds} \right) - m^2 \left( \frac{1}{sH} + \frac{s}{2H^3} \right) \right] \psi^m &= \frac{2s}{H^3} \frac{m}{\tilde{\omega}} \psi^m, \end{aligned} \quad (1.3)$$

which can also be cast into the standard form,

$$\frac{d^2}{ds^2} \psi^m + \frac{1}{sH^2} \frac{d}{ds} \psi^m - \left( \frac{m^2 (H^2 + 1)}{2s^2 H^2} + \frac{2m}{\tilde{\omega} H^2} \right) \psi^m = 0. \quad (1.4)$$

All coefficients in the standard form are rational forms of cylindrical radius  $s$ . The poles of the coefficients give the *singularities* of the equation. These singularities are  $s = 0$  (at the axis) and  $s = 1$  ( $H = 0$ , at the equator), and as will be seen in other case studies, these are the same for all cases presented. Note  $H = (1-s)^{1/2}(1+s)^{1/2}$ . Therefore, a denominator in the form of  $s^a H^b$  produces an  $a$ -th order pole  $s = 0$ , and an  $\frac{b}{2}$ -th order pole  $s = 1$ . An integer  $b$  that is odd produces an *essential singularity* at  $s = 1$ .

Recalling the properties of ODEs, an  $n$ -th order ODE

$$\frac{d^n y}{dx^n} + \sum_{k=0}^{n-1} a_k(x) \frac{d^k y}{dx^k} = 0$$

admits regular solutions in the vicinity of  $x = x_0$  so long as the following quantities are analytic:

$$(x - x_0)^k a_{n-k}(x), \quad k = 0, 1, \dots, n-1.$$

In other words,  $a_{n-k}(x)$  is allowed to have a pole up to the  $k$ -th order. For the second-order ODE above,  $a_1$  has simple poles at  $s = 0$  and  $s = 1$ , and  $a_0$  has a second-order pole at  $s = 0$ , a simple pole at  $s = 1$ . Therefore, all singular points of the coefficients are merely *regular singular points* of the equation, or *apparent singularities*, and the existence of regular solution is guaranteed.

### 1.1.3 Analytical solution

The hydrodynamic equation (1.3) has known analytical solutions. The eigenvalues are given by

$$\tilde{\omega}_n^m = \omega_n^m = \frac{-m}{(n+1)(2n+2m+3) + \frac{m}{2} + \frac{m^2}{4}}, \quad \psi_n^m(s) = s^m H^3 P_n^{(\frac{3}{2}, m)}(2s^2 - 1), \quad n \in \mathbb{Z}^*. \quad (1.5)$$

This is a rare case where the eigenvalue and eigenfunction can be obtained in closed form. These eigenmodes are the inertial modes. Forming a complete (and orthonormal) set in the appropriate Hilbert space, they provide a basis for the streamfunction in the columnar ansatz. The current implementation of the PG model uses these as the radial spectral basis for  $\psi^m(s)$ .

The analytical solution also indicates that the linear operator

$$\frac{H^3}{s} \left[ \frac{d}{ds} \left( \frac{s}{H} \frac{d}{ds} \right) - \frac{m^2}{sH} \right] = (1 - s^2) \frac{d^2}{ds^2} + \frac{1}{s} \frac{d}{ds} - m^2 \frac{1 - s^2}{s^2}$$

has eigenvalues  $\lambda'_n = -2(n+1)(2n+2m+3) - m$ , with corresponding eigenfunctions  $\psi_n^m$  as stated above.

### 1.1.4 System spectrum

The problem is solved numerically using the spectral PG code `PlesioGeostroPy` for several  $m$ .

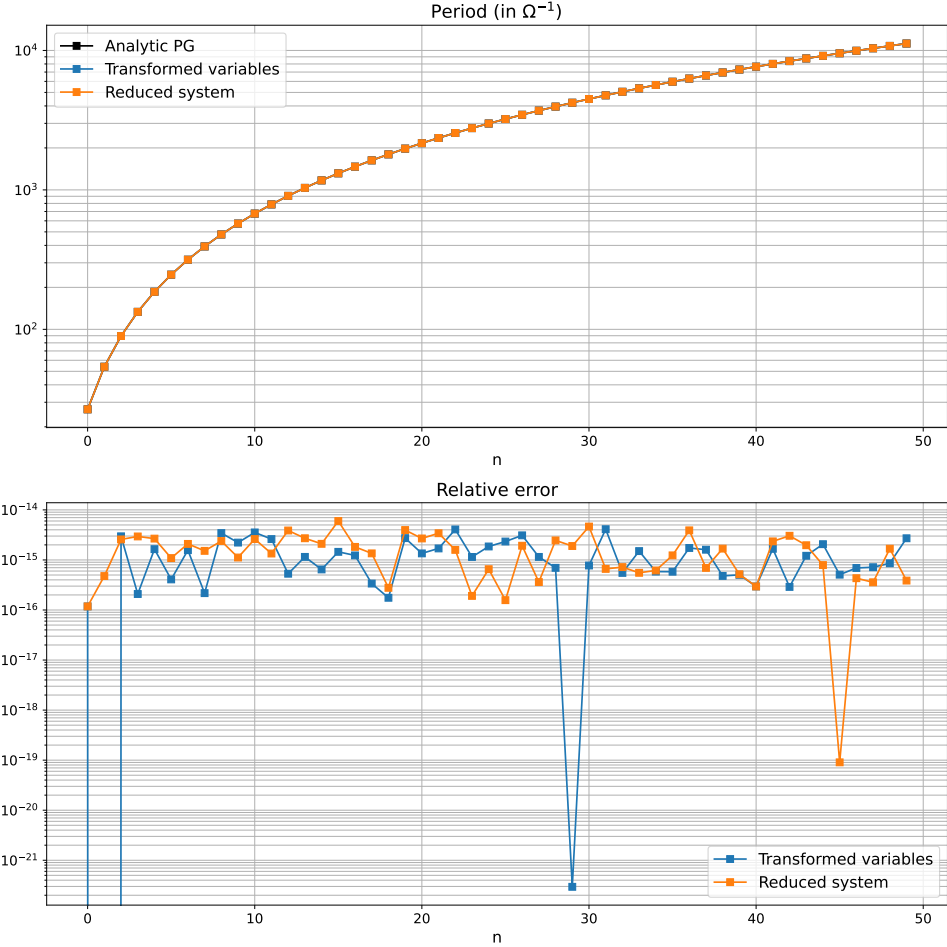


Figure 1.1: Eigenperiods for  $m = 3$  modes solved using transformed variables and reduced system, with analytic solutions. Lower panel shows the relative error compared to analytical solutions.

The eigenvalues for  $m = 3$  eigenmodes are presented in Fig.(1.1). The quadratures are computed in double precision, and the matrices are inserted into a double precision eigensolver. Both the results

of the full system (Transformed variables) and the reduced system are presented. These are both solved using a truncation level of 50 for the streamfunction  $\psi$ .

All hydrodynamic eigenmodes, or inertial modes in the PG model, are eastwards modes (Fig.1.2). As expected from physical arguments, the real parts of the numerically solved eigenvalues are close to machine precision from zero (Fig.1.2). The very small discrepancy from the analytical values (unanimously lower than  $10^{-14}$ , lower panel of Fig.1.1) indicates that all 51 eigenvalues are solved satisfactorily close to machine precision. This is unsurprising since the spectral basis used for the streamfunction is nothing but the analytical eigenmodes, yielding perfect convergence. For this very simple problem, there is virtually no difference between the eigenvalues solved using reduced system or full system, as both are virtually accurate down to machine precision.

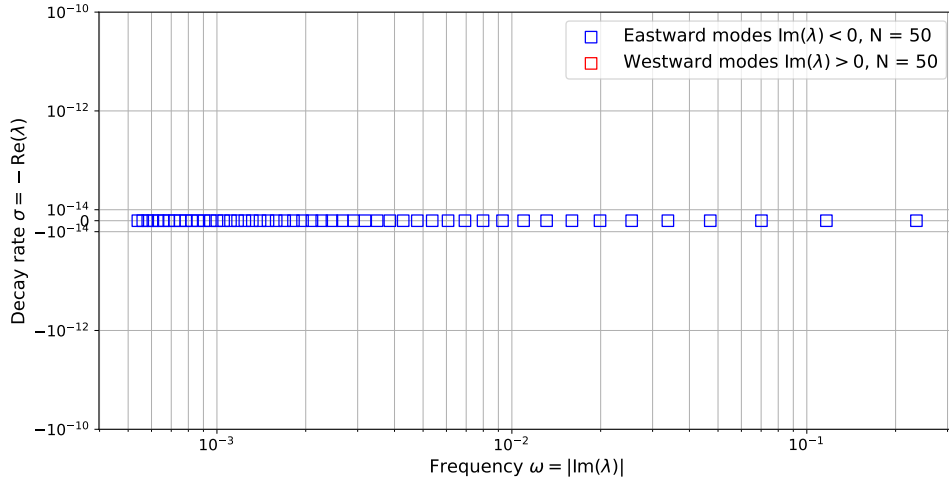


Figure 1.2: Complex spectrum of the  $m = 3$  eigenvalues.

Taking a step back, the eigenperiods of the fundamental ( $n = 0$ ), 2nd-, 5th- and 9th-order modes are shown in Fig.(1.3) as a function of azimuthal wavenumber  $m$ . This is basically a reproduction of Fig.(4.1) in Holdenried-Chernoff (2021) and Fig.(1) in Jackson and Maffei (2020), except the current plot shows numerically solved eigenperiods, while the plots in the cited ones are probably just analytical solutions.

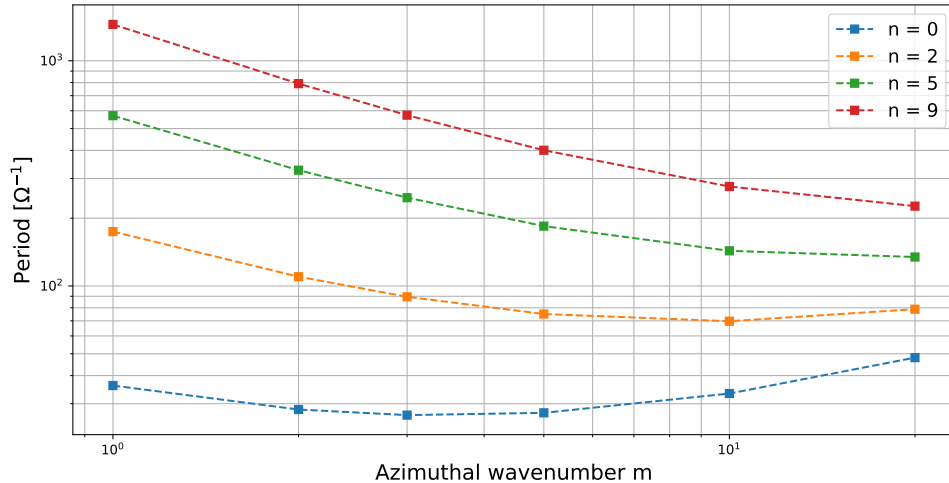


Figure 1.3: Periods as a function of azimuthal wavenumber for different order modes.

There is a discrepancy between the Jackson and Maffei (2020) periods and the Holdenried-Chernoff (2021) periods. The former one is mostly likely missing a  $2\pi$  factor, while the latter one is consistent with

the numerical results presented here. The shortest eigenperiod is observed in the fundamental mode for  $m = 3$ , which has a period of circa 26.7 days. The eigenperiods of all azimuthal wavenumbers increase with higher orders.

### 1.1.5 Selected eigenmodes

The hydrodynamic eigenmodes are pure and simple. As mentioned, they take the analytical form

$$\psi^{mn} = s^{|m|} H^3 P_n^{(\frac{3}{2}, |m|)}(2s^2 - 1) e^{im\phi}.$$

Several eigenmodes are visualized and their spectra shown below. For simplicity, only the results solved using the reduced system are used. However, we have already seen from the eigenvalue comparisons that the full system yields virtually the same solution, at least in this simple eigenvalue problem.

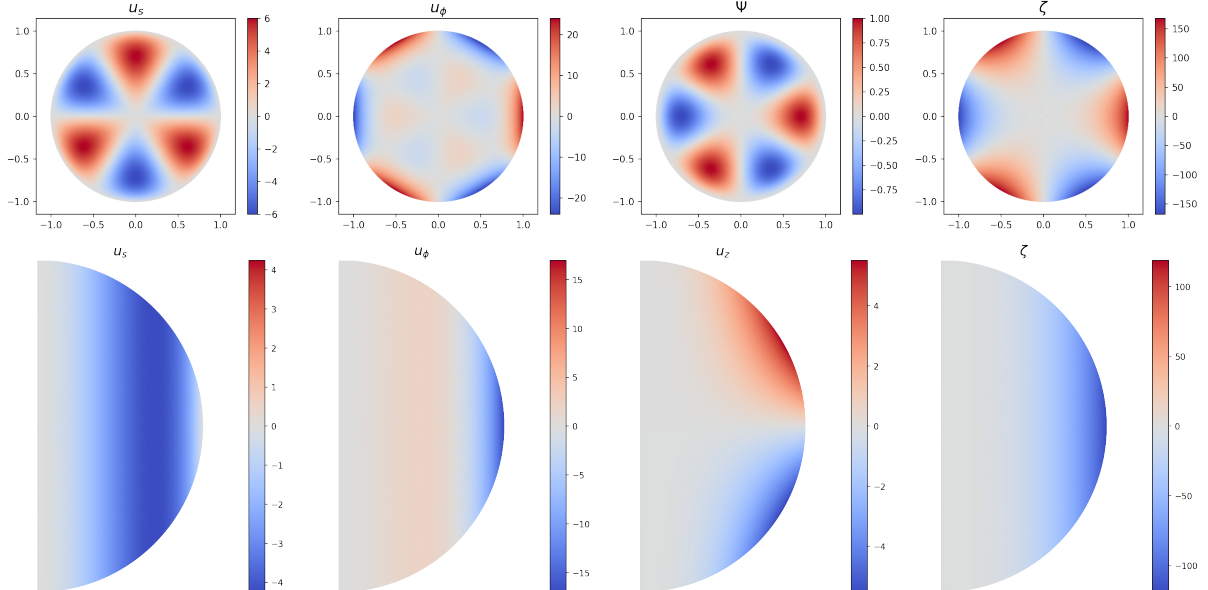


Figure 1.4: Fundamental ( $n = 0$ ) hydrodynamic eigenmode for  $m = 3$ . The upper panel and the lower panel show the equatorial ( $z = 0$ ) and meridional ( $\phi = \pi/4$ ) slices, respectively.

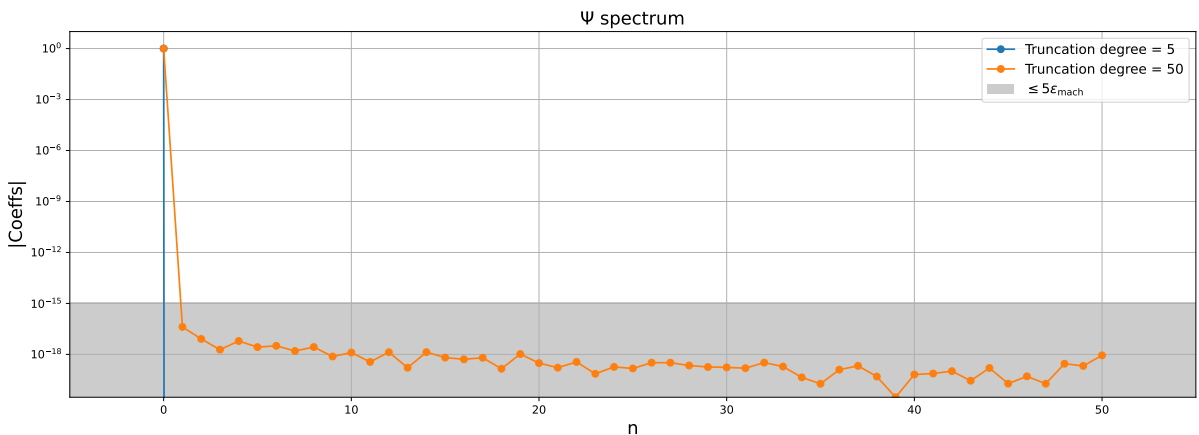


Figure 1.5: Fundamental  $m = 3$  eigenmode streamfunction spectrum at different truncation levels.

The fundamental and the 10-th eigenmode for azimuthal wavenumber  $m = 3$  are visualized in Figs.(1.4) and (1.6), respectively. The visualized amplitude is normalized such that the streamfunction

$\psi$  has amplitude unity in the equatorial plane. Even in the fundamental mode, we see that the azimuthal velocity near the equator is much stronger than any components anywhere else. This is even more exaggerated for higher order modes. As a result, the vorticity is also increasingly concentrated near the equator for higher order modes. Readers who find this result surprising should read section 1.4 of the Ingredients document, where the analytical bases for velocity components as well as vorticity are derived. The analytical bases show that higher order basis function for  $\psi$  translates to strong azimuthal velocity and concentrated vorticity at the equator.

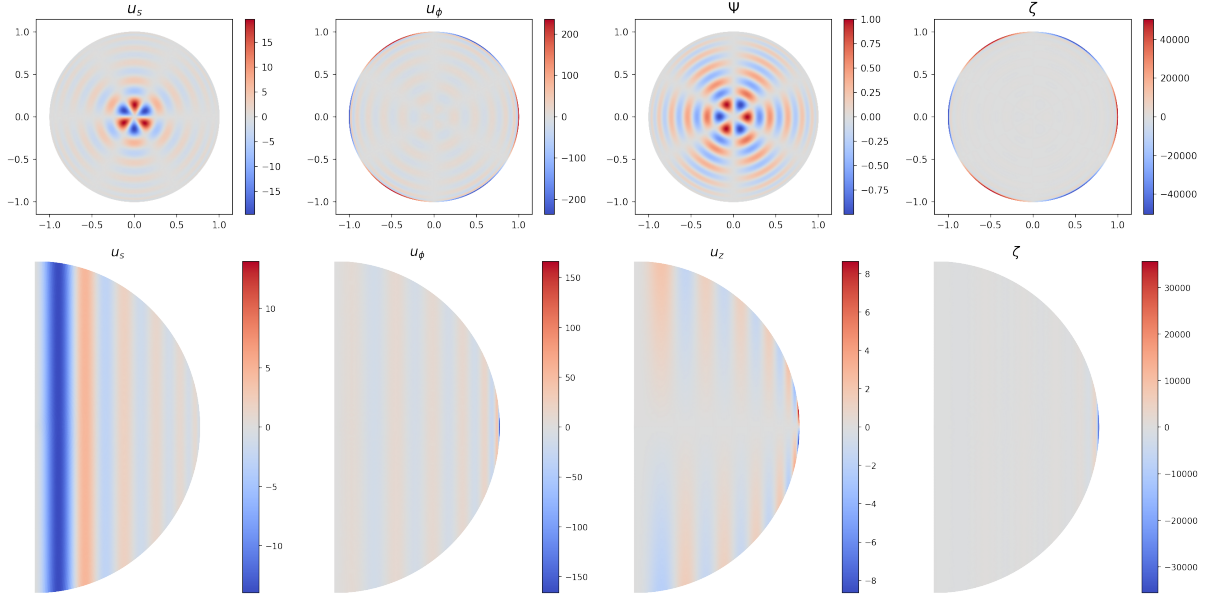


Figure 1.6: 10-th hydrodynamic eigenmode for  $m = 3$ . The upper panel and the lower panel show the equatorial ( $z = 0$ ) and meridional ( $\phi = \pi/4$ ) slices, respectively.

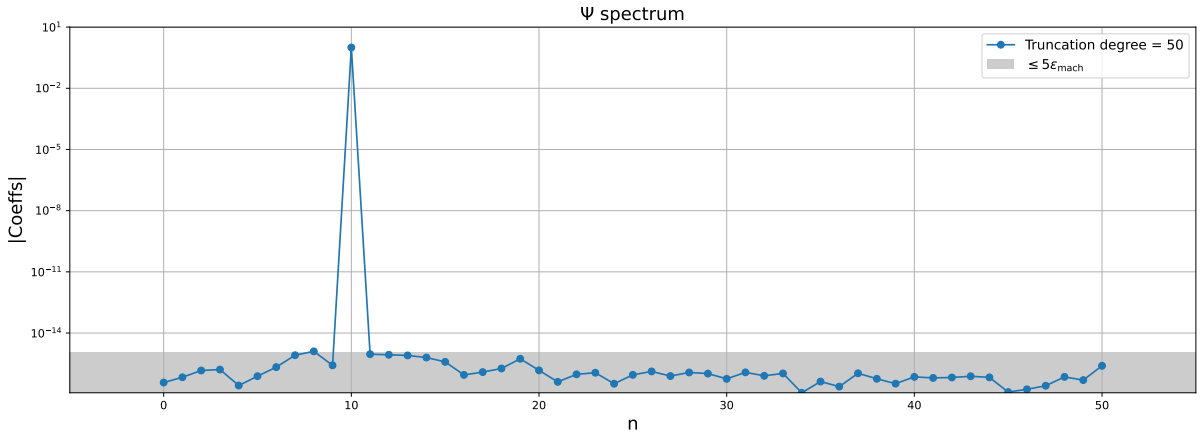


Figure 1.7: 10-th  $m = 3$  eigenmode streamfunction spectrum.

As alluded to, the eigenmodes coincide with the spectral basis (or rather the other way around: the spectral basis comes from the hydrodynamic eigenmodes). This means that the spectrum will contain only spikes at selected basis, as is the case in Figs.(1.5) and (1.7). The fundamental and 10-th eigenmode only has nontrivial coefficient corresponding to the 0-th and the 10-th spectral basis, while all other coefficients are within 5 times machine precision from zero. The result is that the convergence is perfect, meaning as soon as the necessary basis is included within the truncation level, the problem is exactly solvable.

## 1.2 Ideal eigenmodes under Malkus background field

The background field is given by

$$\mathbf{B}^0 = s\hat{\phi}$$

translating to the following background PG quantities:

$$\begin{aligned}\overline{M}_{\phi\phi}^0 &= 2s^2H \\ \widetilde{zM}_{\phi\phi}^0 &= s^2H^2 \\ B_{\phi}^{0e} &= s \\ B_{\phi}^{0+} &= s \\ B_{\phi}^{0-} &= s \\ \Psi^0 &= \overline{M}_{ss}^0 = \overline{M}_{s\phi}^0 = \widetilde{M}_{sz}^0 = \widetilde{M}_{\phi z}^0 = \widetilde{zM}_{ss}^0 = \widetilde{zM}_{s\phi}^0 = 0 \\ B_s^{0e} &= B_z^{0e} = B_{s,z}^{0e} = B_{\phi,z}^{0e} = B_s^{0+} = B_z^{0+} = B_s^{0-} = B_z^{0-} = 0\end{aligned}\tag{1.6}$$

### 1.2.1 Linearized equations

In the Fourier domain (ansatz  $\psi = \psi(s)e^{i\tilde{\omega}t+im\phi} = \psi(s)e^{\lambda t+im\phi}$ ), the set of linearized equations under the Malkus background field reads

$$\begin{aligned}i\tilde{\omega} \left[ \frac{d}{ds} \left( \frac{s}{H} \frac{d}{ds} \right) - m^2 \left( \frac{1}{sH} + \frac{s}{2H^3} \right) \right] \psi &= \frac{2ims}{LeH^3} \psi \\ + \frac{im}{2H} \left( \frac{d\overline{m}_{ss}}{ds} - \frac{d\overline{m}_{\phi\phi}}{ds} \right) + \frac{im}{2sH} (\overline{m}_{ss} - \overline{m}_{\phi\phi}) - \frac{s}{2H} \frac{d^2\overline{m}_{s\phi}}{ds^2} - \frac{3}{2H} \frac{d\overline{m}_{s\phi}}{ds} - \frac{m^2}{2Hs} \overline{m}_{s\phi} \\ - \frac{ims}{2H^2} \frac{d\widetilde{m}_{sz}}{ds} + \frac{m^2}{2H^2} \widetilde{m}_{\phi z} - \frac{im}{2H^2} \widetilde{m}_{sz} - \frac{ims^2}{H^2} b_{\phi}^e - \frac{2s^2}{H^2} b_s^e \\ - \frac{s^3}{2H^2} \left( \frac{db_s^+}{ds} + \frac{db_s^-}{ds} \right) + \left( -\frac{3s^2}{2H^2} - \frac{s^4}{2H^4} \right) (b_s^+ + b_s^-) - \frac{s^2}{2H} \left( \frac{db_z^+}{ds} - \frac{db_z^-}{ds} \right) - \frac{s}{H} (b_z^+ - b_z^-) \\ i\tilde{\omega} \overline{m}_{\phi\phi} &= -4ims \frac{d\psi}{ds} \\ i\tilde{\omega} \overline{m}_{s\phi} &= -2m^2 \psi \\ i\tilde{\omega} \widetilde{m}_{\phi z} &= \frac{m^2 s}{H} \psi \\ i\tilde{\omega} \widetilde{z} \overline{m}_{\phi\phi} &= -2ims H \frac{d\psi}{ds} \\ i\tilde{\omega} \widetilde{z} \widetilde{m}_{s\phi} &= -m^2 H \psi \\ i\tilde{\omega} b_s^e &= -\frac{m^2}{sH} \psi \\ i\tilde{\omega} b_{\phi}^e &= -\frac{im}{H} \frac{d\psi}{ds} \\ \overline{m}_{ss} &= \widetilde{z} \overline{m}_{ss} = \widetilde{m}_{sz} = b_z^e = b_{s,z}^e = b_{\phi,z}^e = 0\end{aligned}\tag{1.7}$$

with induction equations at the boundary given by

$$\begin{aligned}i\tilde{\omega} b_s^+ &= i\tilde{\omega} b_s^- = -\frac{m^2}{sH} \psi \\ i\tilde{\omega} b_{\phi}^+ &= i\tilde{\omega} b_{\phi}^- = -\frac{im}{H} \frac{d\psi}{ds} \\ i\tilde{\omega} b_z^+ &= -i\tilde{\omega} b_z^- = -\frac{m^2}{H^2} \psi.\end{aligned}\tag{1.8}$$

The induction equations in (1.7) and (1.8) have been validated against and are indeed exactly the same as those reported in Holdenried-Chernoff (2021). There is no reference for the streamfunction equation, but its validity can be partially checked when the equation is further reduced into lower dimensions, as shown in the next subsection.

As a final side remark, note that the boundary magnetic terms in the momentum equation (1.7) either consist of sums of or differences between the upper boundary and the lower boundary terms, as a result of the symmetry of the background field with respect to the equatorial plane. The same parity leads to the boundary terms as dictated by (1.8) to be either odd or even functions. The overall outcome is that the boundary terms cancel each other out, and have no effects in the system whatsoever. Although not explicitly pointed out in Holdenried-Chernoff (2021), the original implementation in **Mathematica** ignores the contribution of the boundary terms, but nevertheless yields the correct output. This is most likely due to the fact that the boundary terms play no role anyway in the Malkus model.

### 1.2.2 Standard ODE form

The Malkus field, despite its complicated momentum equation, has a particularly simple reduced form. The 2-order form of the dynamical system takes the following form,

$$\begin{aligned} i\tilde{\omega} \left(1 - \frac{m^2}{\tilde{\omega}^2}\right) \left[ \frac{d}{ds} \left( \frac{s}{H} \frac{d}{ds} \right) - m^2 \left( \frac{1}{sH} + \frac{s}{2H^3} \right) \right] \psi &= 2i \left( \frac{m}{Le} - \frac{m^2}{\tilde{\omega}} \right) \frac{s}{H^3} \psi \\ \left[ \frac{d}{ds} \left( \frac{s}{H} \frac{d}{ds} \right) - m^2 \left( \frac{1}{sH} + \frac{s}{2H^3} \right) \right] \psi &= 2 \frac{\frac{1}{Le} m \tilde{\omega} - m^2}{\tilde{\omega}^2 - m^2} \frac{s}{H^3} \psi \end{aligned} \quad (1.9)$$

which only differs from the hydrodynamic case (1.3) by a factor.

$$\frac{d^2}{ds^2} \psi + \frac{1}{sH^2} \frac{d\psi}{ds} + \frac{m}{m^2 - \tilde{\omega}^2} \frac{1}{2s^2 H^2} \left( \frac{4\tilde{\omega}s^2}{Le} + m(m^2 - \tilde{\omega}^2)(s^2 - 2) - 4ms^2 \right) \psi = 0$$

At the current stage, this form really doesn't seem to yield more information than the fact that both  $s = 0$  and  $s = 1$  are regular singularities of the equation, and regular solutions should exist.

### 1.2.3 Analytical solution

As the ODE in  $\psi$  only differs from eq.(1.3) by a factor, the Malkus background field also inherits the analytical solution from the hydrodynamic case. The analytical eigenvalues are calculated from

$$\frac{\frac{1}{Le} m \tilde{\omega} - m^2}{\tilde{\omega}^2 - m^2} = \frac{m}{\omega_{\text{hydro}}^{mn}}$$

### 1.3 Ideal eigenmodes under toroidal quadrupolar background field

The background field is given by

$$\mathbf{B}^0 = \gamma r \sin \theta (1 - r^2) \hat{\phi} = \gamma s (1 - s^2 - z^2) \hat{\phi}$$

which translates to the following background PG quantities

$$\begin{aligned} \overline{M}_{\phi\phi}^0 &= \frac{16}{15} \gamma^2 s^2 H^5 \\ \widetilde{zM}_{\phi\phi}^0 &= \frac{1}{3} \gamma^2 s^2 H^6 \\ B_{\phi}^{0e} &= \gamma s H^2 \\ \Psi^0 &= \overline{M}_{ss}^0 = \overline{M}_{s\phi}^0 = \overline{M}_{sz}^0 = \overline{M}_{\phi z}^0 = \widetilde{zM}_{ss}^0 = \widetilde{zM}_{s\phi}^0 \\ &= B_z^{0e} = B_s^{0e} = B_{s,z}^{0e} = B_{\phi,z}^{0,e} = B_s^{0\pm} = B_{\phi}^{0\pm} = B_z^{0\pm} = 0. \end{aligned} \quad (1.10)$$

#### 1.3.1 Linearized equations

Under the toroidal quadrupolar background field, the streamfunction equation takes the form,

$$\begin{aligned} i\tilde{\omega} \left[ \frac{d}{ds} \left( \frac{s}{H} \frac{d}{ds} \right) - m^2 \left( \frac{1}{sH} + \frac{s}{2H^3} \right) \right] \psi &= \frac{2ims}{LeH^3} \psi \\ + \frac{im}{2H} \frac{d\overline{m}_{ss}}{ds} + \frac{im}{2sH} \overline{m}_{ss} - \frac{im}{2H} \frac{d\overline{m}_{\phi\phi}}{ds} - \frac{im}{2sH} \overline{m}_{\phi\phi} - \frac{s}{2H} \frac{d^2 \overline{m}_{s\phi}}{ds^2} - \frac{3}{2H} \frac{d\overline{m}_{s\phi}}{ds} - \frac{m^2}{2sH} \overline{m}_{s\phi} \\ - \frac{ims}{2H^2} \frac{d\widetilde{m}_{sz}}{ds} - \frac{im}{2H^2} \widetilde{m}_{sz} + \frac{m^2}{2H^2} \widetilde{m}_{\phi z} + 2\gamma \frac{s^2(2s^2-1)}{H^2} b_s^e - i\gamma ms^2 b_\phi^e. \end{aligned} \quad (1.11)$$

The magnetic quantities are described by the induction equations in the PG model, which are given by

$$\begin{aligned} i\tilde{\omega} \overline{m}_{\phi\phi} &= -i \frac{32}{15} \gamma^2 m \left[ sH^4 \frac{d\psi}{ds} - 2s^2 H^2 \psi \right] \\ i\tilde{\omega} \overline{m}_{s\phi} &= -\frac{16}{15} \gamma^2 m^2 H^4 \psi \\ i\tilde{\omega} \widetilde{m}_{\phi z} &= \frac{1}{3} \gamma^2 m^2 sH^3 \psi \\ i\tilde{\omega} \widetilde{z m}_{\phi\phi} &= -i \frac{2}{3} \gamma^2 m \left[ sH^5 \frac{d\psi}{ds} - 2s^2 H^3 \psi \right] \\ i\tilde{\omega} \widetilde{z m}_{s\phi} &= -\frac{1}{3} \gamma^2 m^2 H^5 \psi \\ i\tilde{\omega} b_s^e &= -\gamma m^2 \frac{H}{s} \psi \\ i\tilde{\omega} b_\phi^e &= -i\gamma m \left[ H \frac{d\psi}{ds} - \frac{2s}{H} \psi \right] \\ \overline{m}_{ss} &= \widetilde{m}_{sz} = \widetilde{z m}_{ss} = b_z^e = b_{s,z}^e = b_{\phi,z}^e = 0 \end{aligned} \quad (1.12)$$

The boundary induction equations are all trivial; all components vanish at the boundary:

$$b_s^\pm = b_\phi^\pm = b_z^\pm = 0. \quad (1.13)$$

The streamfunction has been validated by comparing the hand-derived result and the symbolic engine result. All the PG induction equations are validated against and are exactly the same as in Holdenried-Chernoff (2021). The fact that magnetic perturbations vanish at the boundary is a direct consequence of vanishing background field at the boundary. Therefore, I am confident that these equations are valid.

### 1.3.2 Standard ODE form

To check the regularity of the system, we form the standard ODE of  $\psi$  as a function of  $s$  by merging the PG equations and boundary induction equations into one single ODE (1.19). The standard form is a second order equation in  $\psi$ .

$$\begin{aligned} & \left( -\frac{8}{15} \gamma^2 m^2 s H^4 + \omega^2 s \right) \frac{d^2 \psi}{ds^2} \\ & + \left( \frac{\gamma^2 m^2}{15} H^2 (25s^2 - 8) + \frac{\omega^2}{H^2} \right) \frac{d\psi}{ds} \\ & + \left( -\frac{2}{15} \gamma^2 m^2 s H^2 - \frac{\gamma^2 m^4}{30} \frac{H^2 (11s^2 - 16)}{s} + \frac{\omega^2 m^2 (s^2 - 2)}{2H^2 s} - \frac{2}{Le} \frac{\omega m s}{H^2} \right) \psi = 0 \end{aligned} \quad (1.14)$$

Amazingly, this is identical to eq.(5.41) in Holdenried-Chernoff (2021).

The 3-nd order term has a simple pole at  $s = 0$  and a simple pole at  $s = 1$ ;

The 2-nd order term has a 2-nd order pole at  $s = 0$  and a 2-nd order pole at  $s = 1$ ;

The 1-st order term has a 3-rd order pole at  $s = 0$  and a 3-rd order pole at  $s = 1$ ;

The 0-th order term has a 4-th order pole at  $s = 0$  and a 3-rd order pole at  $s = 1$ .

The overall conclusion is that the singularities of the equation are both regular singularities, so regular solutions should exist.

## 1.4 Ideal eigenmodes under poloidal dipolar background field

The background field is given by

$$\mathbf{B}^0 = -6sz\hat{\mathbf{s}} + (12s^2 + 6z^2 - 10)\hat{\mathbf{z}}$$

which translates to the following background PG quantities

$$\begin{aligned}\overline{M_{ss}}^0 &= 24H^3 s^2 \\ \widetilde{M_{sz}}^0 &= -18H^4 s + 2H^2 (-36s^3 + 30s) \\ \widetilde{zM_{ss}}^0 &= 18H^4 s^2 \\ B_z^{0e} &= 12s^2 - 10 \\ B_{s,z}^{0e} &= -6s \\ B_s^{0+} &= -6Hs \\ B_z^{0+} &= 6s^2 - 4 \\ B_s^{0-} &= 6Hs \\ B_z^{0-} &= 6s^2 - 4 \\ \Psi^0 &= \overline{M_{\phi\phi}}^0 = \overline{M_{s\phi}}^0 = \widetilde{M_{\phi z}}^0 = \widetilde{zM_{\phi\phi}}^0 = \widetilde{zM_{s\phi}}^0 = 0 \\ B_s^{0e} &= B_\phi^{0e} = B_{\phi,z}^{0e} = B_\phi^{0+} = B_\phi^{0-} = 0.\end{aligned}\tag{1.15}$$

### 1.4.1 Linearized equations

As always, the most complicated part is the streamfunction equation. Under the poloidal dipolar background field, it takes the form,

$$\begin{aligned}i\tilde{\omega} \left[ \frac{d}{ds} \left( \frac{s}{H} \frac{d}{ds} \right) - m^2 \left( \frac{1}{sH} + \frac{s}{2H^3} \right) \right] \psi &= \frac{2ims}{LeH^3} \psi \\ &+ \frac{im}{2H} \frac{dm_{ss}}{ds} + \frac{im}{2Hs} \overline{m_{ss}} - \frac{im}{2H} \frac{dm_{\phi\phi}}{ds} - \frac{im}{2Hs} \overline{m_{\phi\phi}} - \frac{s}{2H} \frac{d^2 \overline{m_{s\phi}}}{ds^2} - \frac{3}{2H} \frac{d \overline{m_{s\phi}}}{ds} - \frac{m^2}{2sH} \overline{m_{s\phi}} \\ &- \frac{ims}{2H^2} \frac{dm_{sz}}{ds} - \frac{im}{2H^2} \widetilde{m_{sz}} + \frac{m^2}{2H^2} \widetilde{m_{\phi z}} + 4ims \frac{6s^2 - 5}{H^2} b_z^e - 2s^2 \frac{6s^2 - 5}{H^2} b_{\phi,z}^e \\ &+ \frac{2s}{H} \left( \frac{db_\phi^+}{ds} - \frac{db_\phi^-}{ds} \right) + \frac{2}{H} (b_\phi^+ - b_\phi^-) + \frac{ims}{H^2} (b_z^+ + b_z^-) + \frac{im(s^2 - 2)}{H^3} (b_s^+ - b_s^-).\end{aligned}\tag{1.16}$$

The magnetic quantities are described by the induction equations in the PG model, which are given by

$$\begin{aligned}
i\tilde{\omega}\overline{m_{ss}} &= i48m \left[ sH^2 \frac{d\psi}{ds} + (4s^2 - 2)\psi \right] \\
i\tilde{\omega}\overline{m_{s\phi}} &= 24 \left[ -s^2 H^2 \frac{d^2\psi}{ds^2} + s(1 - 2s^2) \frac{d\psi}{ds} \right] \\
i\tilde{\omega}\overline{m_{sz}} &= i6m \left[ \frac{12s^4 - 19s^2 + 7}{H} \frac{d\psi}{ds} - \frac{54s^4 - 57s^2 + 14}{sH} \psi \right] \\
i\tilde{\omega}\overline{m_{\phi z}} &= 6 \left[ sH(9s^2 - 7) \frac{d^2\psi}{ds^2} + \frac{1}{H}(2s^2 - 1)(9s^2 - 7) \frac{d\psi}{ds} \right] \\
i\tilde{\omega}\overline{zm_{ss}} &= i36m \left[ sH^3 \frac{d\psi}{ds} + 2H(2s^2 - 1)\psi \right] \\
i\tilde{\omega}\overline{zm_{s\phi}} &= 18 \left[ -s^2 H^3 \frac{d^2\psi}{ds^2} + sH(1 - 2s^2) \frac{d\psi}{ds} \right] \\
i\tilde{\omega}b_z^e &= i2m \frac{6s^2 - 7}{H^3} \psi \\
i\tilde{\omega}b_{s,z}^e &= i6m \left[ -\frac{1}{H} \frac{d\psi}{ds} + \frac{2(1 - 2s^2)}{sH^3} \psi \right] \\
i\tilde{\omega}b_{\phi,z}^e &= 6 \left[ \frac{s}{H} \frac{d^2\psi}{ds^2} + \frac{2s^2 - 1}{H^3} \frac{d\psi}{ds} \right] \\
\overline{m_{\phi\phi}} &= \overline{zm_{\phi\phi}} = b_s^e = b_\phi^e = 0
\end{aligned} \tag{1.17}$$

All the PG induction equations are validated against and are exactly the same as in Holdenried-Chernoff (2021). In contrast, the boundary induction equations are given as follows

$$\begin{aligned}
i\tilde{\omega}b_s^+ &= -i\tilde{\omega}b_s^- = i6m \left[ -\frac{d\psi}{ds} + \frac{2(1 - 2s^2)}{sH^2} \psi \right], \\
i\tilde{\omega}b_\phi^+ &= -i\tilde{\omega}b_\phi^- = 6 \left[ s \frac{d^2\psi}{ds^2} + \frac{2s^2 - 1}{H^2} \frac{d\psi}{ds} \right], \\
i\tilde{\omega}b_z^+ &= i\tilde{\omega}b_z^- = i2m \left[ \frac{3s}{H} \frac{d\psi}{ds} + \frac{4(3s^2 - 1)}{H^3} \psi \right].
\end{aligned} \tag{1.18}$$

While the meridional components  $b_s^\pm$  and  $b_z^\pm$  share the same expression as in Holdenried-Chernoff (2021), the azimuthal components  $b_\phi^\pm$  are not mentioned in the previous work. It is unclear what argument was made to ignore this boundary term, but the calculation here seems to suggest that this component is however not trivial. Is this used or not in the previously obtained results? This is a question that only the original author can answer.

We see that contrary to the boundary fields for Malkus field, the boundary fields for the poloidal dipolar background field has another parity. The equatorial components  $b_s$  and  $b_\phi$  are opposite at the upper and the lower boundary, while the vertical component  $b_z$  matches. This means that the boundary terms in (1.16) do not cancel out like they do in (1.7), and thus boundary terms do matter.

### 1.4.2 Standard ODE form

To check the regularity of the system, we form the standard ODE of  $\psi$  as a function of  $s$  by merging the PG equations and boundary induction equations into one single ODE (1.19). The standard form is a 4-th order system in  $\psi$ . The singularities of the equations are  $s = 0$ , i.e. at the axis, and  $H = 0$  ( $s = 1$ ), i.e. at

the equator. The singularities of the coefficients are analyzed below.

$$\begin{aligned}
& \frac{d^4\psi}{ds^4} + \frac{8 - 9s^2}{sH^2} \frac{d^3\psi}{ds^3} \\
& + \left( \frac{\omega^2}{12H^2s^2} + \frac{-m^2(s^4 - 5s^2 + 4) - 16s^2 + 20}{4s^2H^4} \right) \frac{d^2\psi}{ds^2} \\
& + \left( \frac{\omega^2}{12s^3H^4} + \frac{-m^2(s^6 - 2s^4 - 2s^2 + 3) + 18s^6 - 51s^4 + 41s^2 - 5}{s^3H^6} \right) \frac{d\psi}{ds} \\
& + \left( \frac{\omega^2m^2(s^2 - 2)}{24s^4H^4} - \frac{1}{Le} \frac{\omega m}{6s^2H^4} - \frac{m^2 \cdot (30s^6 - 127s^4 + 156s^2 - 32)}{4s^4H^6} \right) \psi = 0
\end{aligned} \tag{1.19}$$

The 3-rd order term has a simple pole at  $s = 0$  and a simple pole at  $s = 1$ ;

The 2-nd order term has a 2-nd order pole at  $s = 0$  and a 2-nd order pole at  $s = 1$ ;

The 1-st order term has a 3-rd order pole at  $s = 0$  and a 3-rd order pole at  $s = 1$ ;

The 0-th order term has a 4-th order pole at  $s = 0$  and a 3-rd order pole at  $s = 1$ .

The overall conclusion is that the singularities of the equation are both regular singularities, so regular solutions should exist. However, singularity aside, these coefficients differ from the ones as provided in Holdenried-Chernoff (2021). Some coefficients are the same, but not all. Recalling that in the previous work, the  $b_\phi^\pm$  may be ignored, I tried to remove these equations before assembling the 2-nd order ODE. The result is as follows

$$\begin{aligned}
& \frac{d^4\psi}{ds^4} + \frac{6 - 9s^2}{sH^2} \frac{d^3\psi}{ds^3} \\
& + \left( \frac{\omega^2}{12s^2H^2} + \frac{m^2(-s^4 + 5s^2 - 4) - 16s^2 + 12}{4s^2H^4} \right) \frac{d^2\psi}{ds^2} \\
& + \left( \frac{\omega^2}{12s^3H^4} + \frac{-m^2(s^6 - 2s^4 - 2s^2 + 3) + 18s^6 - 47s^4 + 31s^2 - 3}{s^3H^6} \right) \frac{d\psi}{ds} \\
& + \left( \frac{\omega^2m^2(s^2 - 2)}{24s^4H^4} - \frac{1}{Le} \frac{\omega m}{6s^2H^4} - \frac{m^2 \cdot (30s^6 - 127s^4 + 156s^2 - 32)}{4s^4H^6} \right) \psi = 0
\end{aligned} \tag{1.20}$$

Now the first three coefficients all match with Holdenried-Chernoff (2021). However, the coefficients of the lowest two order terms still do not match. The only difference, as it seems, lies in the terms containing  $m^2$  in these coefficients. It does not seem to be possible to tell the right from wrong here, so a thorough symbolic re-analysis seems necessary.

One notable feature that might aid debugging is that according to the equations presented here, there aren't even terms that can give  $s^7$  on the numerator. However, both discrepant coefficients contain  $s^7m^2$  terms in Holdenried-Chernoff (2021). "Dimension" analysis of the streamfunction equation (1.16) seems to indicate that such a high degree is not possible. If something is wrong with the derivation, the mistake may have already occurred at eq.(1.16). Understanding how this  $s^7$  term comes about might be a key to finding out potential errors.

#### 1.4.3 System spectrum

#### 1.4.4 Selected eigenmodes

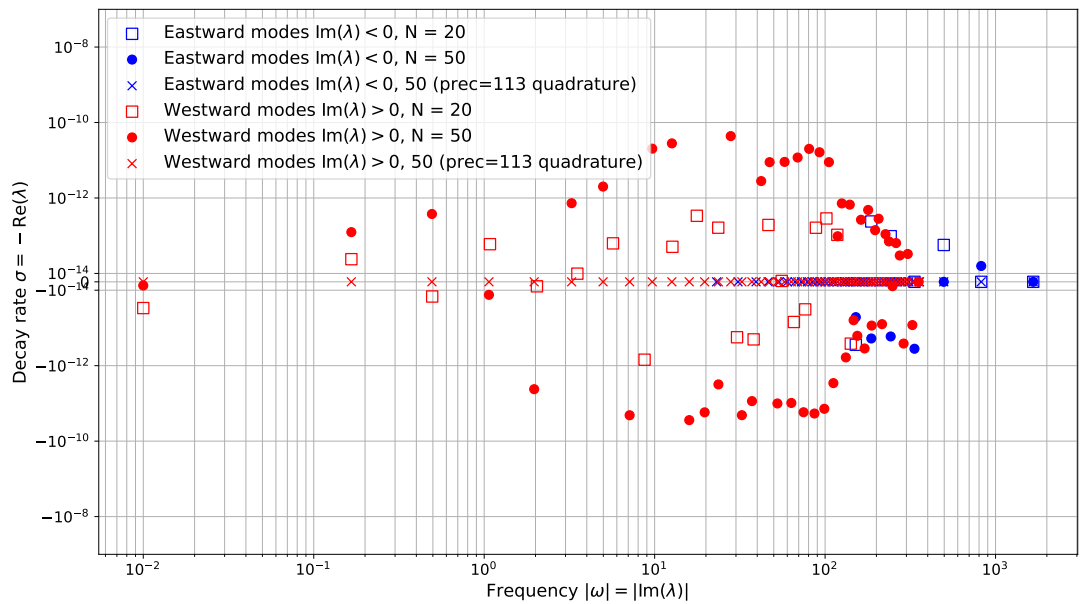


Figure 1.8: Spectrum for  $m = 3$  modes.

## 1.5 Ideal eigenmodes under SL2N1, a quadrupolar poloidal magnetic field

The background field, which we call SL2N1, is defined as

$$\mathbf{B}^0 = \nabla \times \nabla \times \left( ar^2 5(r^2 - 7) \mathbf{r} \right) = \gamma s \left( -5s^2 - 15z^2 + 7 \right) \hat{\mathbf{s}} + 2\gamma z \left( 10s^2 + 5z^2 - 7 \right) \hat{\mathbf{z}}$$

where  $a$  and  $\gamma = \frac{3}{2}\sqrt{\frac{5}{\pi}}a$  are normalisation factors. This is the lowest-degree axisymmetric poloidal mode for spherical harmonic  $l = 2$  that satisfies the vacuum exterior magnetic boundary condition (see the Ingredients document), and will hereinafter be referred to as S-L2N1 (poloidal,  $l = 2$ ,  $n = 1$ ). The field is visualised in Fig. 1.9.

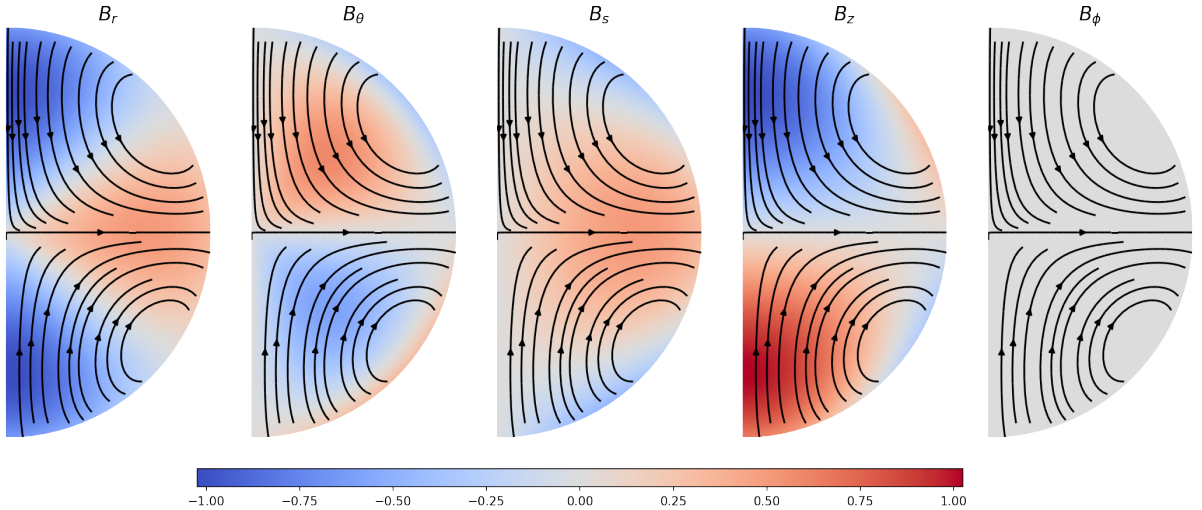


Figure 1.9: The spherical and cylindrical components of the axisymmetric S-L2N1 background field. The plot shows the field for  $a = \frac{1}{4}\sqrt{\frac{3}{26}}$  or  $\gamma = \frac{3}{8}\sqrt{\frac{15}{26\pi}}$ .

The S-L2N1 background field is a new design, and the ideal PG MHD eigenmodes under this background field have never been studied.

### 1.5.1 Linearised equation

The streamfunction equation under the S-L2N1 background field takes the form,

$$\begin{aligned} i\tilde{\omega} \left[ \frac{d}{ds} \left( \frac{s}{H} \frac{d}{ds} \right) - m^2 \left( \frac{1}{sH} + \frac{s}{2H^3} \right) \right] \psi &= \frac{2ims}{\text{Le}H^3} \psi + \frac{im}{2sH} \frac{d(\overline{s m_{ss}})}{ds} - \frac{im}{2sH} \frac{d(\overline{s m_{\phi\phi}})}{ds} \\ &- \frac{s}{2H} \frac{d^2 \overline{m_{s\phi}}}{ds^2} - \frac{3}{2H} \frac{d \overline{m_{s\phi}}}{ds} - \frac{m^2}{2sH} \overline{m_{s\phi}} - \frac{im}{2H^2} \frac{d(\overline{s m_{sz}})}{ds} + \frac{m^2}{2H^2} \overline{m_{\phi z}} \\ &+ \frac{s^2(5s^2 - 7)}{H^2} \frac{d(s b_\phi^e)}{ds} + \frac{im\gamma(s^2 - 2)}{H^2} (b_s^+ + b_s^-) - \frac{im\gamma s^3}{H^3} (b_z^+ - b_z^-) \\ &+ \gamma \frac{6s^4 - 9s^2 + 2}{H^4} (b_\phi^+ + b_\phi^-) + \gamma \frac{s(2 - 3s^2)}{H^2} \left( \frac{db_\phi^+}{ds} + \frac{db_\phi^-}{ds} \right). \end{aligned} \quad (1.21)$$

The magnetic induction equations in the PG model are given by

$$\begin{aligned}
i\tilde{\omega}\overline{m_{ss}} &= 16im\gamma^2 \left[ s \left( 5s^4 - 10s^2 + 6 \right) \frac{d\psi}{ds} + \frac{(25s^6 - 60s^4 + 48s^2 - 12)}{H^2} \psi \right] \\
i\tilde{\omega}\overline{m_{s\phi}} &= \gamma^2 \left[ s^2 \left( -40s^4 + 80s^2 - 48 \right) \frac{d^2\psi}{ds^2} + \frac{s(-80s^6 + 200s^4 - 176s^2 + 48)}{H^2} \frac{d\psi}{ds} \right] \\
i\tilde{\omega}\overline{m_{sz}} &= 2im\gamma^2 \left[ -\frac{25s^6 - 35s^4 + 8s^2 + 4}{H} \frac{d\psi}{ds} + \frac{-125s^8 + 235s^6 - 114s^4 - 10s^2 + 8}{sH^3} \psi \right] \\
i\tilde{\omega}\widetilde{m_{\phi z}} &= \gamma^2 \left[ sH \left( -25s^4 + 5s^2 + 8 \right) \frac{d^2\psi}{ds^2} + \frac{(-50s^6 + 35s^4 + 11s^2 - 8)}{H} \frac{d\psi}{ds} \right] \\
i\tilde{\omega}\widetilde{zm_{ss}} &= 2im\gamma^2 \left[ sH \left( 25s^4 - 40s^2 + 19 \right) \frac{d\psi}{ds} + \frac{125s^6 - 260s^4 + 177s^2 - 38}{H} \psi \right] \\
i\tilde{\omega}\widetilde{zm_{s\phi}} &= \gamma^2 \left[ s^2H \left( -25s^4 + 40s^2 - 19 \right) \frac{d^2\psi}{ds^2} + \frac{s(-50s^6 + 105s^4 - 78s^2 + 19)}{H} \frac{d\psi}{ds} \right] \\
i\tilde{\omega}b_s^e &= im\gamma \left[ \frac{7 - 5s^2}{H} \frac{d\psi}{ds} + \frac{-25s^4 + 41s^2 - 14}{sH^3} \psi \right] \\
i\tilde{\omega}b_\phi^e &= \gamma \left[ \frac{s(5s^2 - 7)}{H} \frac{d^2\psi}{ds^2} + \frac{10s^4 - 19s^2 + 7}{H^3} \frac{d\psi}{ds} \right] \\
\overline{m_{\phi\phi}} &= \widetilde{zm_{\phi\phi}} = b_z^e = b_{s,z}^e = b_{\phi,z}^e = 0
\end{aligned} \tag{1.22}$$

The boundary induction equations read

$$\begin{aligned}
i\tilde{\omega}b_s^+ &= i\tilde{\omega}b_s^- = 2im\gamma \left[ \frac{5s^2 - 4}{H} \frac{d\psi}{ds} + \frac{25s^4 - 32s^2 + 8}{sH^3} \psi \right], \\
i\tilde{\omega}b_\phi^+ &= i\tilde{\omega}b_\phi^- = \gamma \left[ \frac{-10s^3 + 8s}{H} \frac{d^2\psi}{ds^2} + \frac{-20s^4 + 26s^2 - 8}{H^3} \frac{d\psi}{ds} \right], \\
i\tilde{\omega}b_z^+ &= -i\tilde{\omega}b_z^- = 2im\gamma \left[ \frac{s(4 - 5s^2)}{H^2} \frac{d\psi}{ds} + \frac{-25s^4 + 32s^2 - 10}{H^4} \psi \right].
\end{aligned} \tag{1.23}$$

### 1.5.2 Eigenvalue spectrum

The system of PG equations is solved in its canonical form, with normalisation factor for the background field  $a = \frac{1}{4}\sqrt{\frac{3}{26}}$  (or  $\gamma = \frac{3}{8}\sqrt{\frac{15}{26\pi}}$ ). The value is chosen to normalise the  $L^2$ -norm (the energy norm) of the background field, and it also approximately normalises the max-norm to around unity (Fig. 1.9). The full unfiltered eigenvalue spectrum is shown in Fig. 1.10. The eigenvalue spectrum under the S-L2N1 background field shows clear convergence at high eigenfrequency, as well as mild convergence at low eigenfrequency. The spectrum is then filtered using the reciprocal eigenvalue drift criterion, with the threshold for the fast modes being  $10^4$  and the threshold for the slow modes being 30. The eigenvalues classified as converged are shown in the complex plane in Fig. 1.11. The 3-D eigenvalues, computed using the code `MCModes`, are also shown for comparison. The eigenfrequencies of the modified inertial eigenmodes in the PG model follow closely those in 3D. The frequencies of the slow PG modes occupy the same orders of magnitude as the 3-D eigenfrequencies, and are typically within one octave of difference (Fig. 1.12), similar to the S1 case. However, a major difference is that all the "slow" modes are prograde modes, propagating in the same direction as the modified inertial modes (Fig. 1.11). This is completely different from the S1 case, and different from all the 3-D computations I have seen. It is therefore questionable if these are actually the MC modes; even if they are, they would not serve as good approximations of the 3-D columnar MC modes. In addition, in both the 3-D and PG case, the

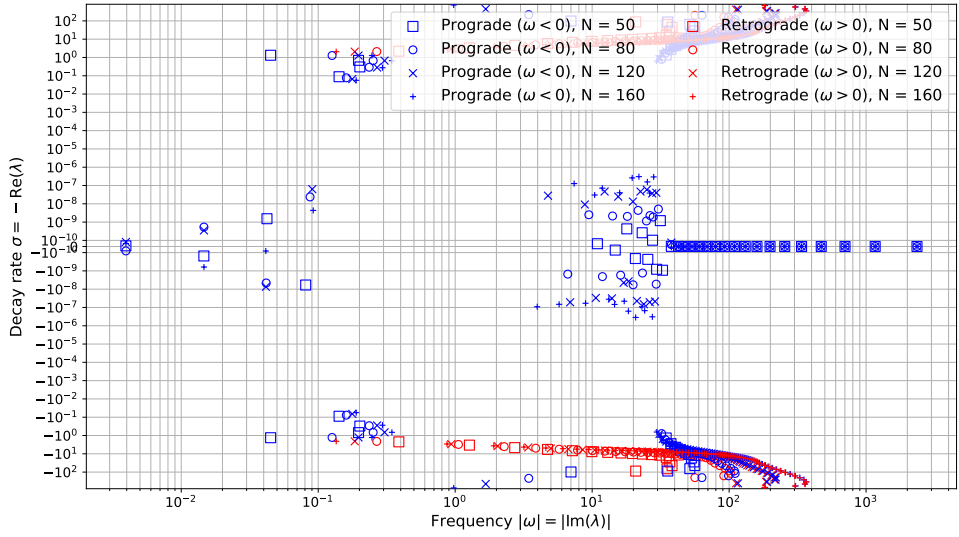


Figure 1.10: Unfiltered full eigenvalue spectrum for the  $m = 3$  eigenvalue problem under S-L2N1 background field. Colours encode the direction of the eigenmode. Different markers encode the eigenvalue solutions from different resolutions.

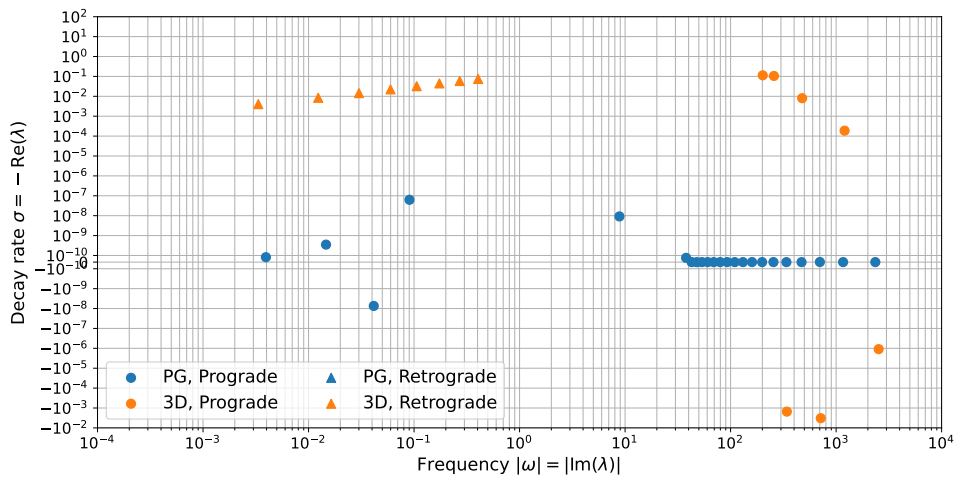


Figure 1.11: Filtered eigenvalue spectra for the  $m = 3$  eigenvalue problem under S-L2N1 background field in the PG and 3D models, solved with  $N = 120$ .

eigenvalue solutions exhibit non-physical real parts. In the 3-D computation, the modified inertial modes occasionally show a considerable positive growth rate, a feature that should be impossible in a diffusive system. In the PG case, the low-frequency eigenvalues exhibit non-trivial (but still very small) real parts as well. It is possible that both phenomena are caused by precision loss during e.g. eigenvalue solver, and hence it might be useful to use higher precision and check if it resolves this issue.

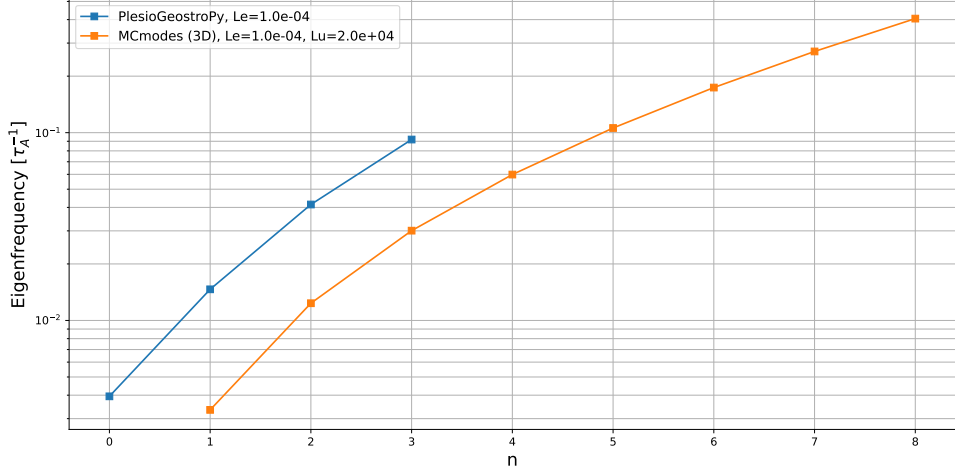


Figure 1.12: Filtered (absolute) eigenfrequencies of the slow modes for the  $m = 3$  eigenvalue problem under S-L2N1 background field in the PG and 3D models, solved with  $N = 120$ .

In summary, under the S-L2N1 background field, the PG model yields modified inertial modes that are very good approximations of their 3-D counterpart in terms of eigenfrequencies. On the other hand, the PG system fails to yield MC modes that approximate well the frequencies and direction of the 3-D columnar MC modes. The slow modes that numerically converge in the PG system, while of the same order of magnitude of frequencies, all show prograde propagation, and likely have a different nature from the 3-D columnar MC modes. It remains to be further investigated whether the existence of such slow modes is purely a numerical error or discrepancy of the system.

### 1.5.3 Selected eigenmodes

Once again, the modified inertial modes not only show good convergence and matching eigenfrequencies in both 3-D and PG calculations, but show coherent eigenmode solutions as well (Fig. 1.13). These eigenmodes in the PG system match well the 3-D counterparts in both spatial structure and amplitudes. The modified inertial modes also boast excellent convergence in the eigenmode spectrum. Even for the 15th modified inertial mode, a resolution of merely  $N = 50$  approximates the coefficients well in the spectral domain (Fig. 1.14).

We have seen that the solved slow PG modes under the S-L2N1 background field are prograde, propagating in a different direction from the 3-D columnar MC modes, and hence have quite different eigenfrequencies. The comparison of the eigenmode structure confirms that the PG slow modes are of drastically different form (Fig. 1.15). The two visualised eigenmodes show almost no resemblance in their radial distribution. While the flow field in 3-D columnar MC modes is mildly concentrated towards the axis, it is completely concentrated near the boundary in the PG slow modes. Accordingly, the induced magnetic fields also show drastic discrepancies.

Curiously enough, the amplitude spectrum shows reasonable convergence for these slow PG modes (Fig. 1.16), and hence the existence of such strange slow modes is not (at least not completely) a numerical problem. The drastic difference of these modes suggests essential difference in the generating mechanism or an essential error in the implementation. It is hence questionable whether such discrepancy can be reconciled by extension of the PG model alone, e.g. by adding magnetic diffusion. While additional

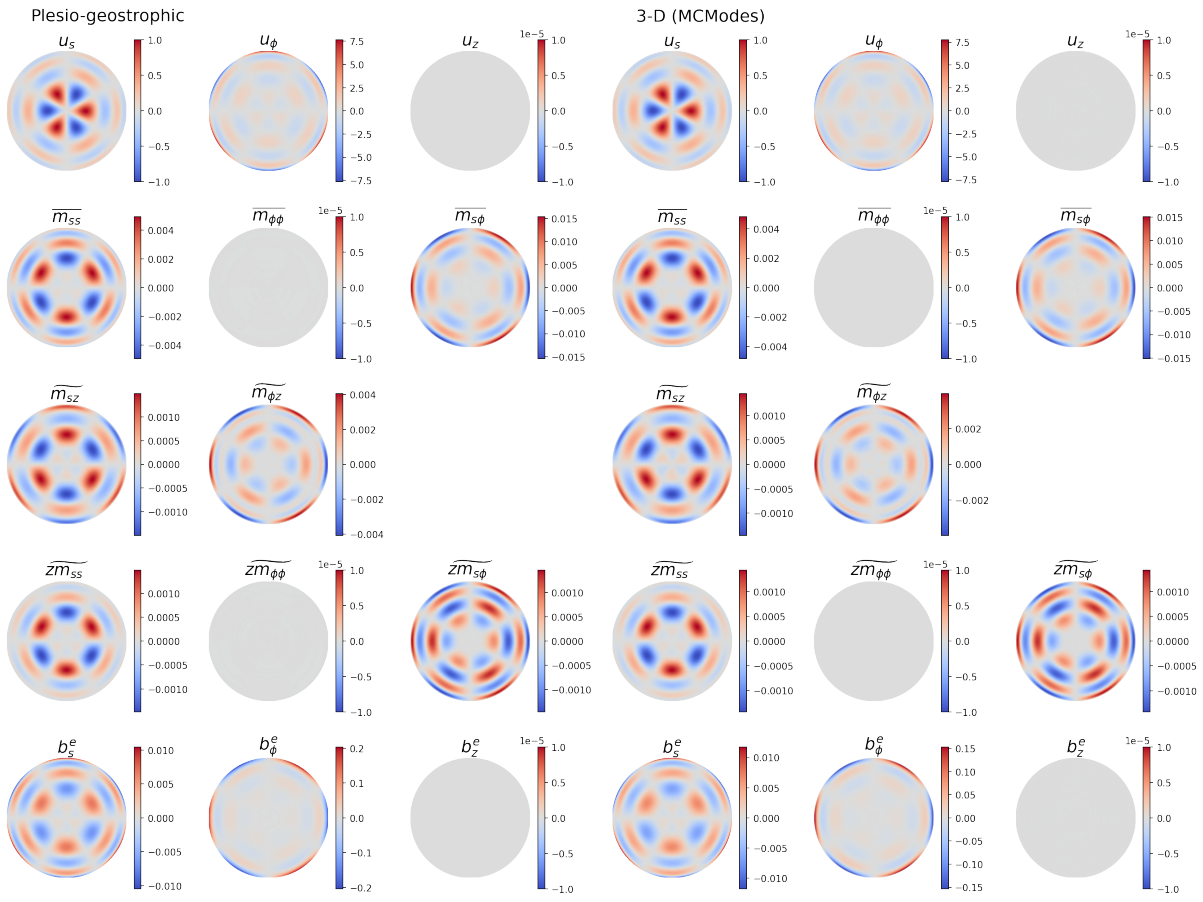


Figure 1.13: Equatorial section of the 3rd modified inertial mode resolved by PG (left) and 3-D (right) models. The integrated quadratic moments of the 3-D case are computed by integrating the vector magnetic field obtained in the 3-D model.

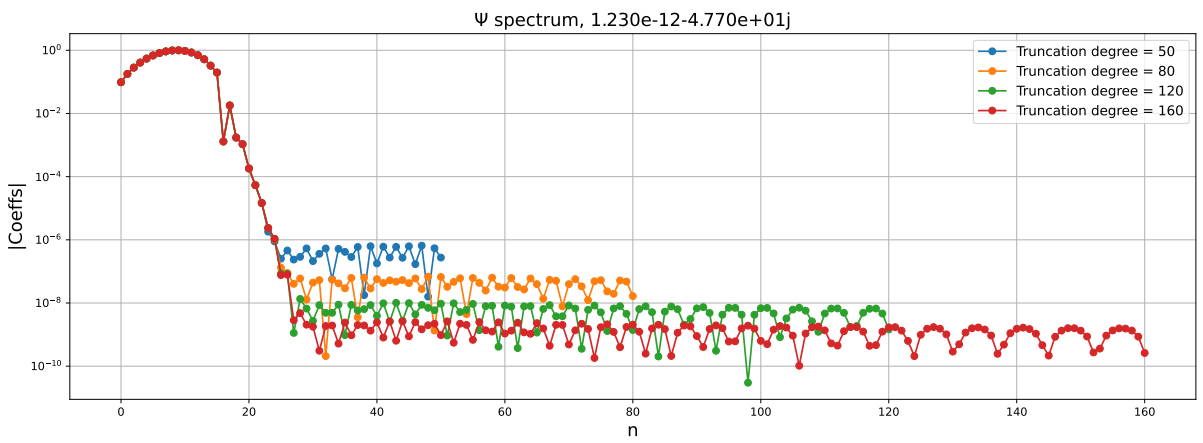


Figure 1.14: Amplitude spectrum of the spectral coefficients for the streamfunction for the 15th PG modified inertial mode solved under different resolutions.

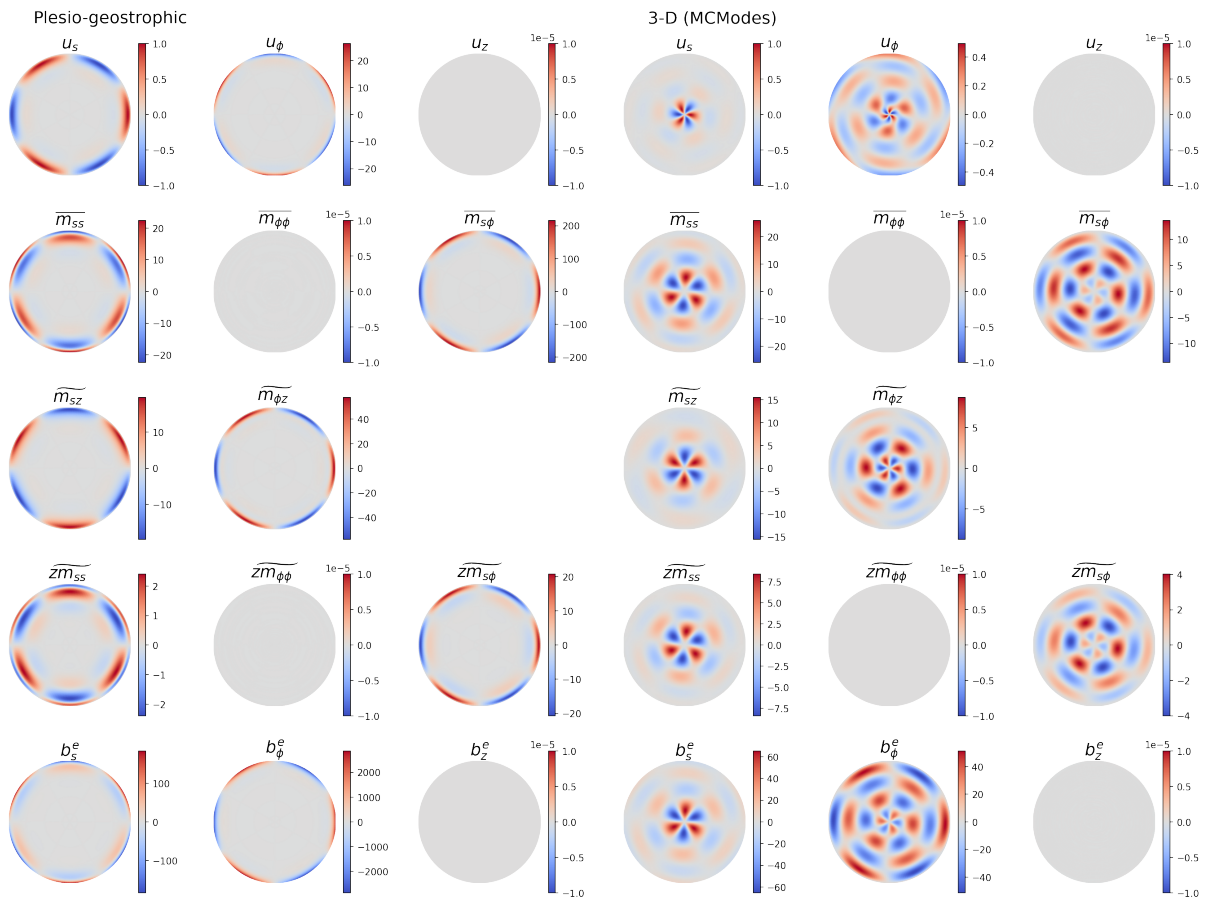


Figure 1.15: Equatorial section of the 3rd slow mode resolved by PG (left) and 3rd columnar MC mode in 3-D (right) models.

components such as diffusion are being appended to the PG system (Part II), I recommend further investigation into the discrepancy of the S-L2N1 slow modes.

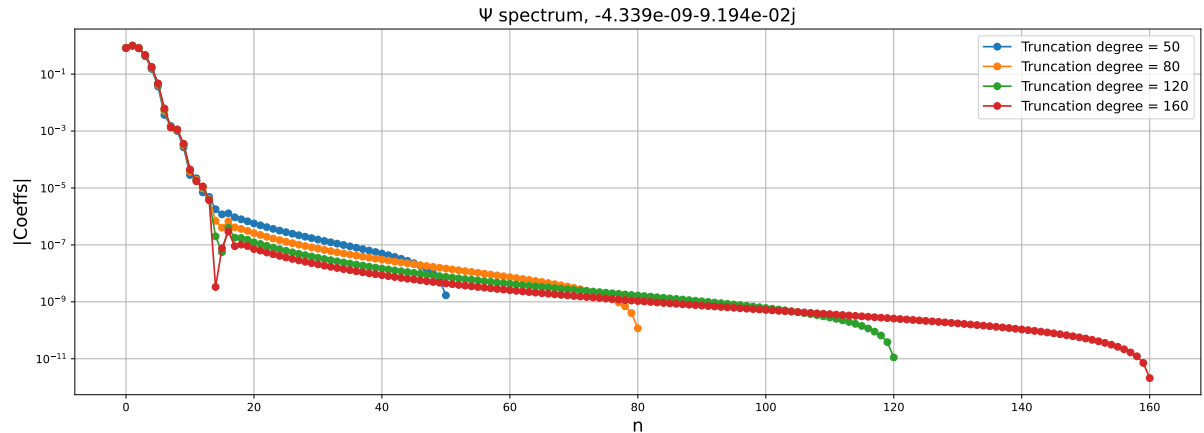


Figure 1.16: Amplitude spectrum of the spectral coefficients for the streamfunction for the 3rd PG slow mode solved under different resolutions.

## 1.6 Ideal eigenmodes under T1-SL2N1, a mixed toroidal-poloidal equatorially symmetric magnetic field

The background field, which we call T1-SL2N1, is defined as

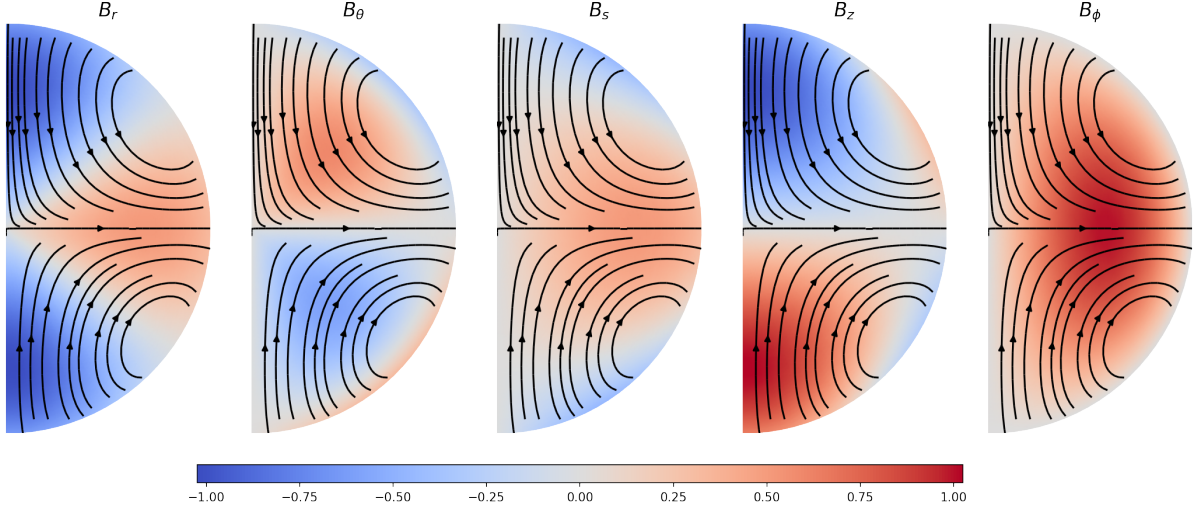


Figure 1.17: Background field T1-SL2N1

This is a background field with purely equatorially symmetric property (i.e. has mirror symmetry with respect to the equatorial plane, also sometimes referred to as "quadrupolar" parity). Background fields T1 and SL2N1 have this symmetry individually, but instead of having either purely poloidal or purely toroidal component, the current background field is a mixture of both poloidal and toroidal fields.

Linearized equations omitted.

### 1.6.1 System spectrum

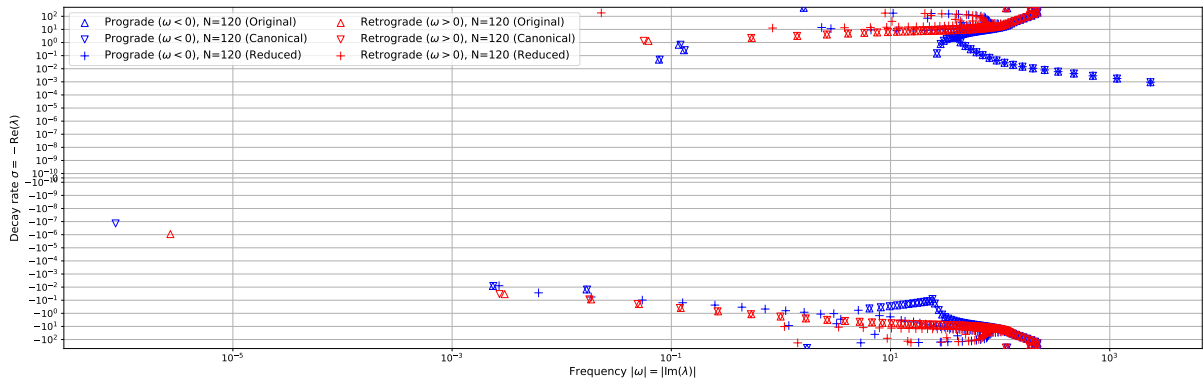
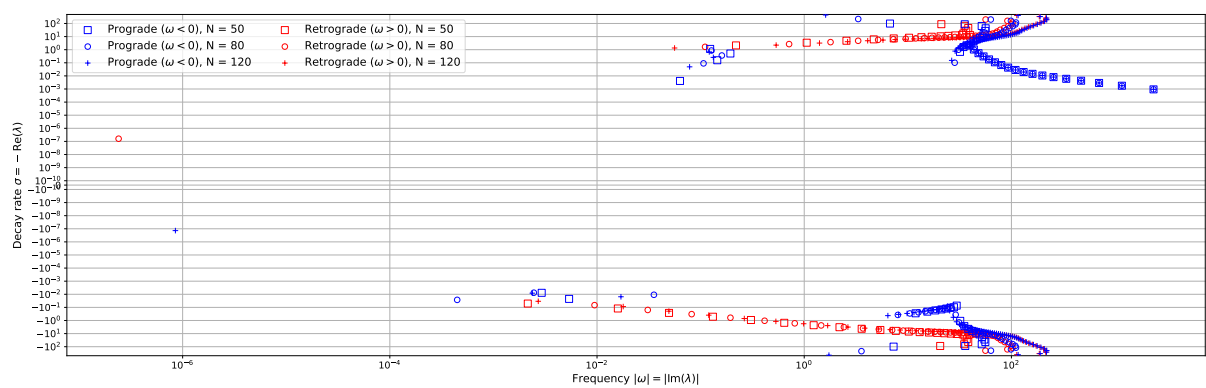


Figure 1.18: Spectrum of three different spectral methods at the same resolution

### 1.6.2 Selected eigenmodes



## 1.7 Ideal eigenmodes under S1-T2, a mixed toroidal-poloidal equatorially anti-symmetric magnetic field

The background field, which we call S1-T2, is defined as

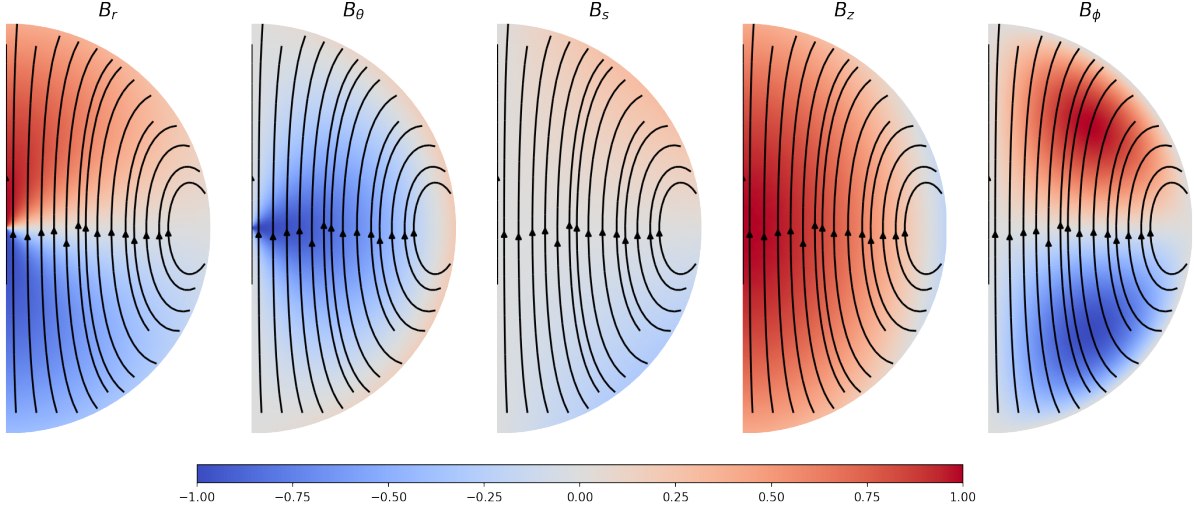


Figure 1.19: Background field T1-SL2N1

This is a background field with purely equatorially anti-symmetric property (i.e. has mirror anti-symmetry with respect to the equatorial plane, also sometimes referred to as "dipolar" parity). Background fields S1 and T2 have this symmetry individually, but instead of having either purely poloidal or purely toroidal component, the current background field is a mixture of both poloidal and toroidal fields.

### 1.7.1 System spectrum

The ideal PG eigenmodes have been calculated under the S1-T2 background field. An example of the resulting unfiltered eigenvalue spectra for Lehnert number  $\text{Le} = 10^{-4}$  and  $m = 3$  is shown in Fig. (1.20) for different formulations, and Fig. (1.21) at different resolutions for each formulation. We see (i) the eigenvalues converge with increasing resolution for all three formulations (Fig. 1.21) as eigenvalues computed under higher resolutions begin to stack on one another, and (ii) such converged eigenvalue solutions are agreed upon by all three formulations (Fig. 1.21). These observations suggest that these converged eigenvalue solutions are a robust feature across all formulations, hence represent physical eigenmodes.

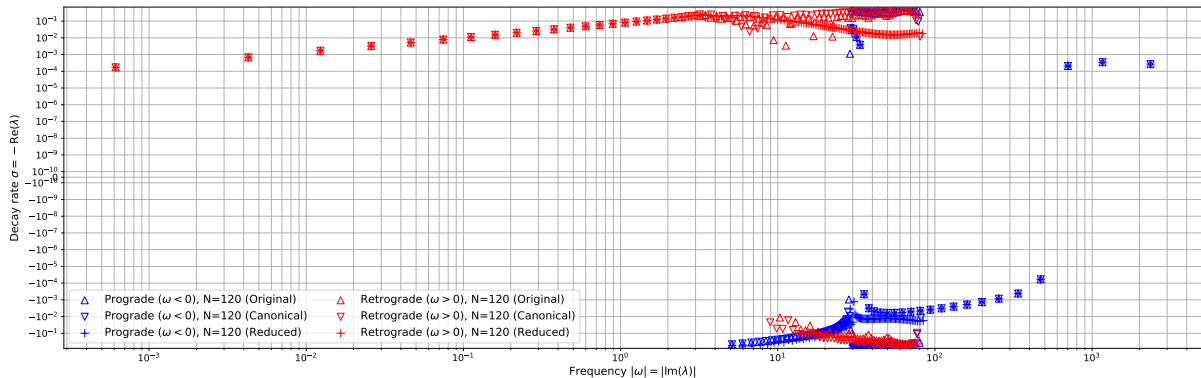


Figure 1.20: Eigenvalue spectra (unfiltered) of three different formulations at the same resolution for Lehnert number  $\text{Le} = 10^{-4}$  and  $m = 3$ .

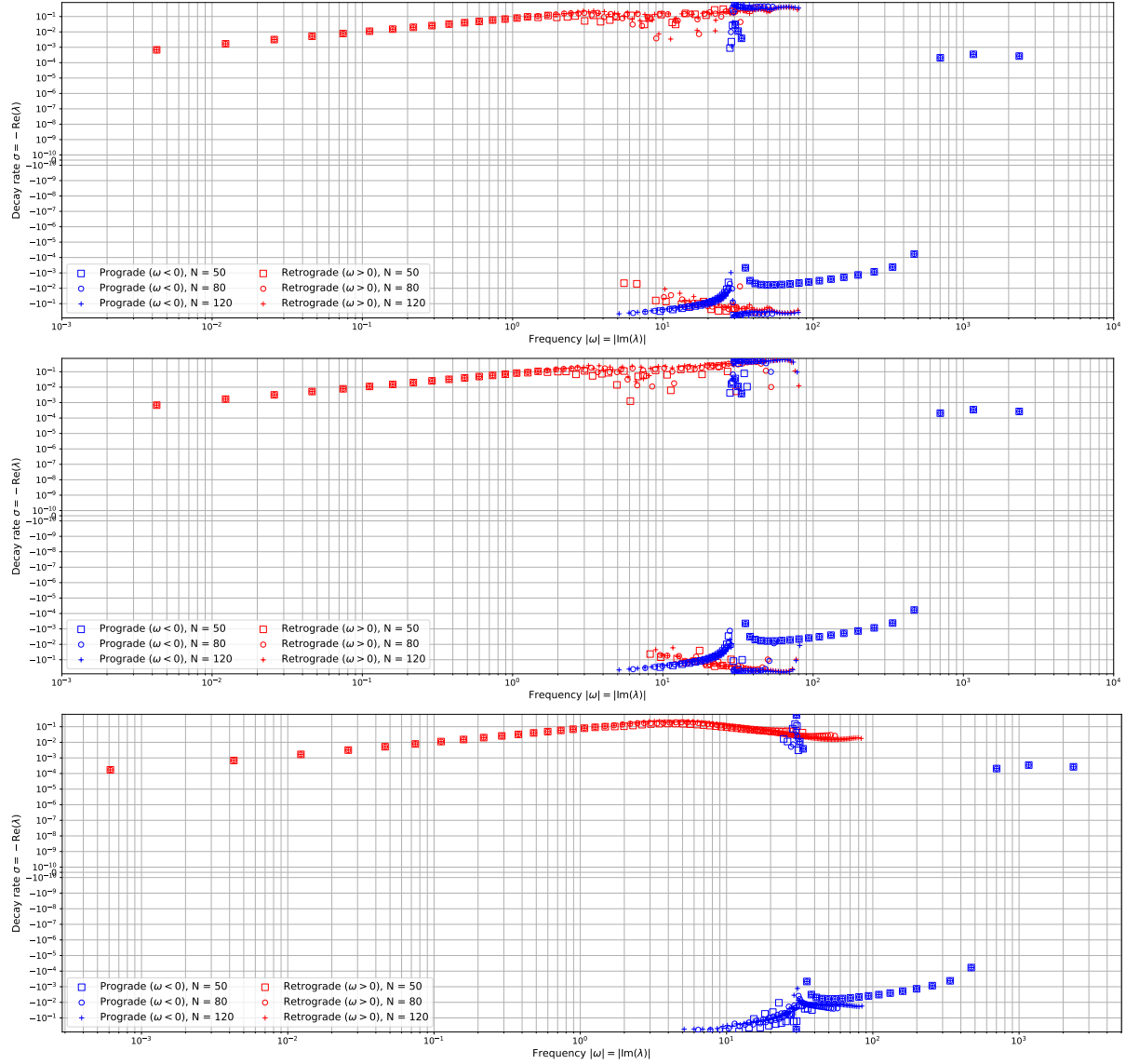


Figure 1.21: Eigenvalue spectra (unfiltered) at different resolutions for the original PG formulation (top), the canonical formulation (middle) and the stream function - forcing ( $\psi$ -F) formulation.

We then proceed with comparing the PG eigenvalues with those in the 3-D calculation. The 3-D calculations are conducted at the same Lehnert number  $Le = 10^{-4}$ , but with  $Lu = 2 \times 10^4$ . The PG results shown hereafter are processed from the canonical formulation. The eigenvalue spectra of the PG eigenvalues are shown in Fig. (1.22).

### 1.7.2 Selected eigenmodes

The 12th modified inertial mode and the 7th (mode with approx. 7 zeros in the cylindrical radius) Magneto-Coriolis mode are visualised in Fig. (1.23) and (1.24), respectively.

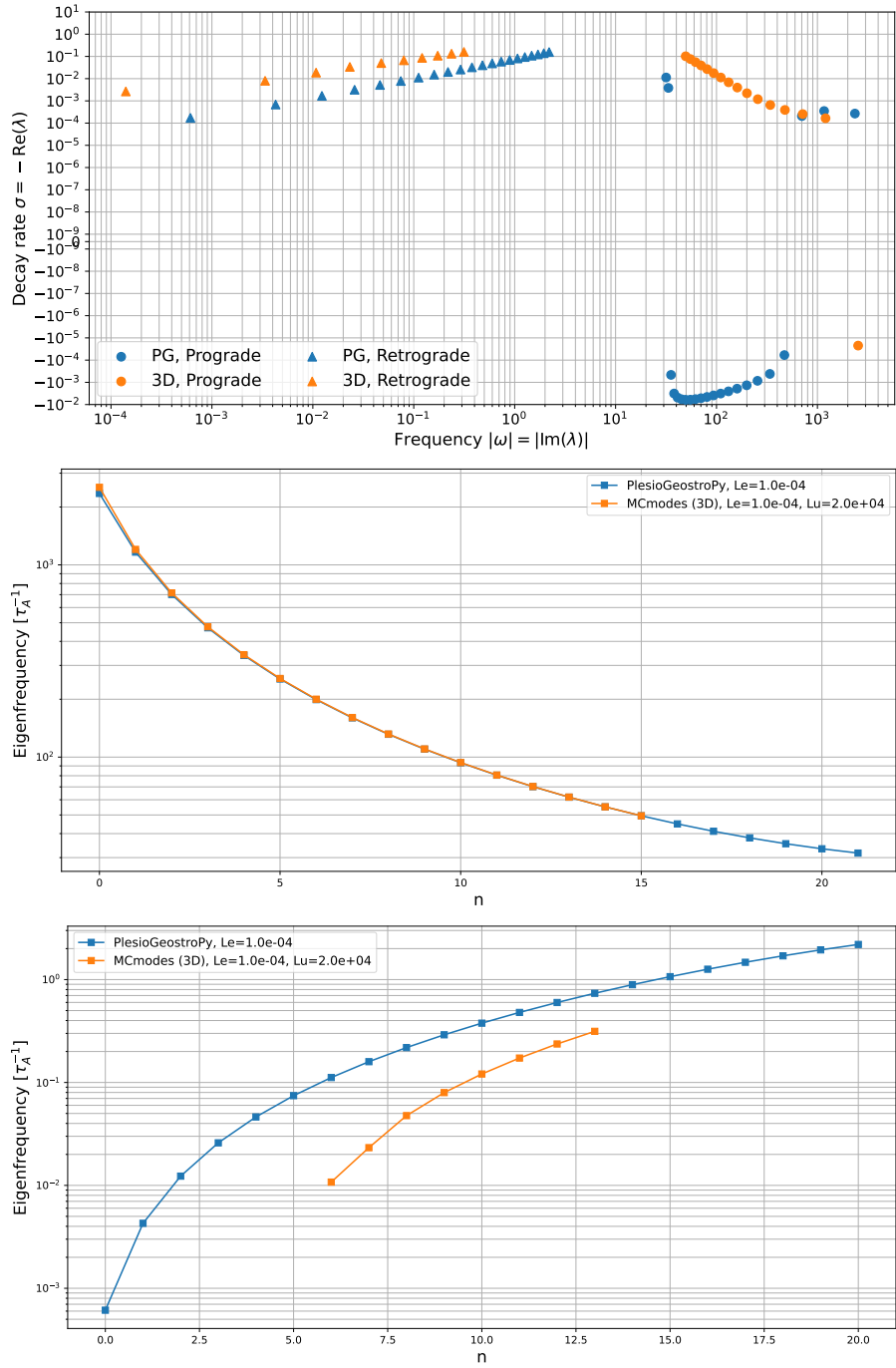


Figure 1.22: Distribution of the converged ideal PG eigenvalues under the S1-T2 background field and their diffusive 3-D counterparts. The figures show the converged eigenspectra on a complex plane (top), the eigenfrequencies as a function of estimated radial zeros for the prograde modes (middle), and for the retrograde modes (bottom).

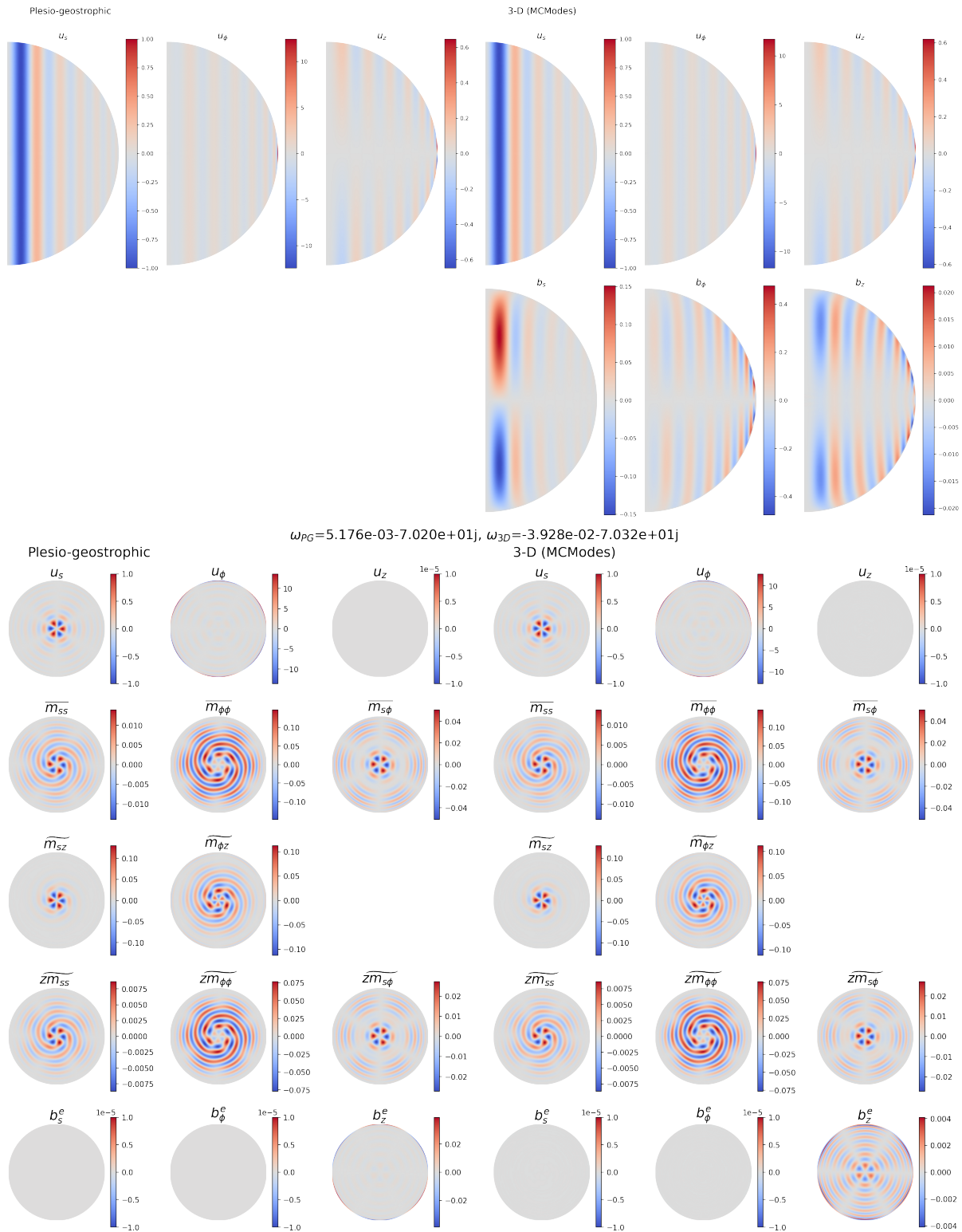


Figure 1.23: Meridional (top plot) and equatorial (lower plot) sections of the 12th modified inertial mode for PG (left columns) and 3-D (right columns) calculation.

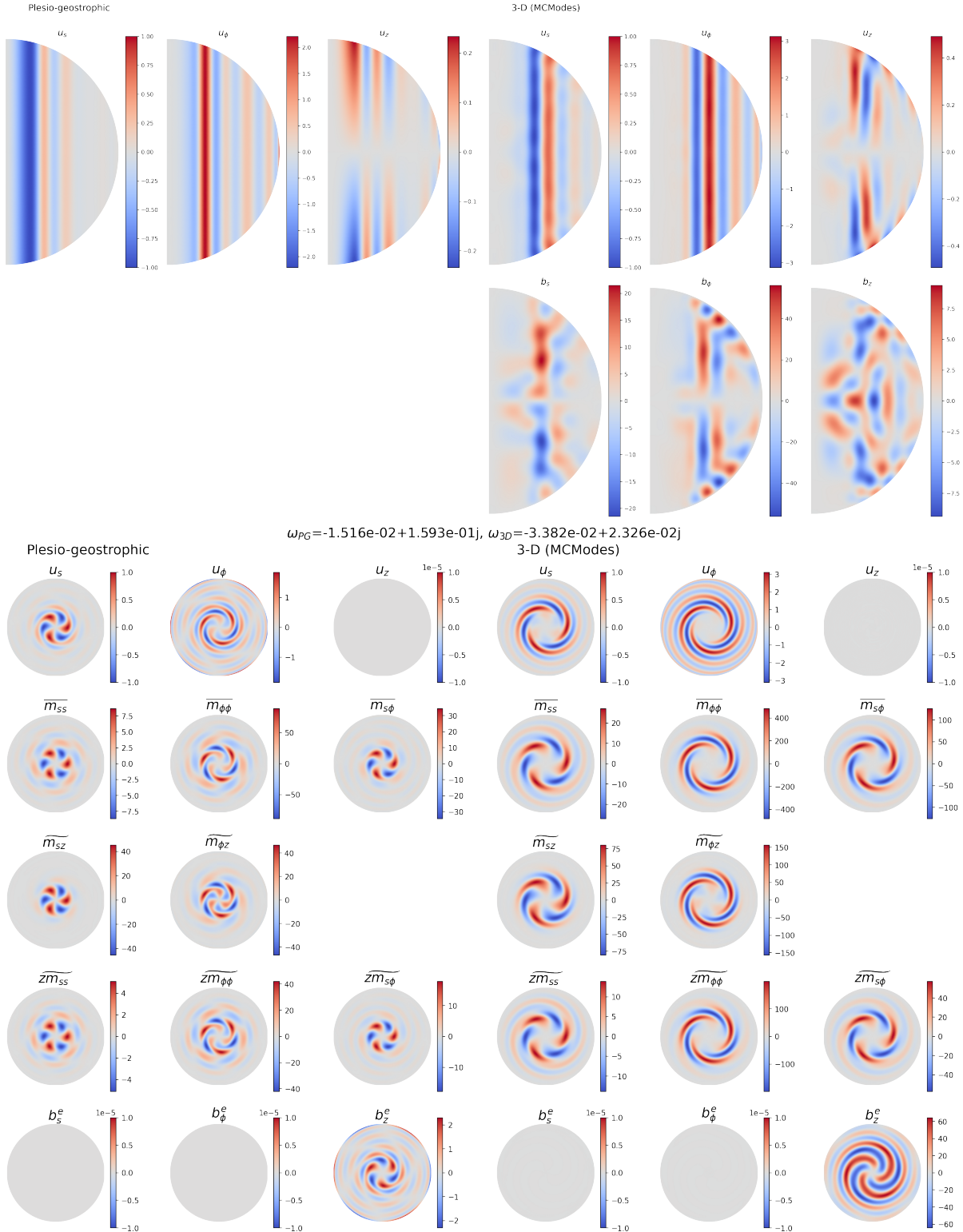


Figure 1.24: Meridional (top) and equatorial (bottom) sections of the Magneto-Coriolis mode with approx. 7 radial zeros for PG (left columns) and 3-D (right columns) calculation.

## Appendix A

### 3-D slow hydromagnetic modes

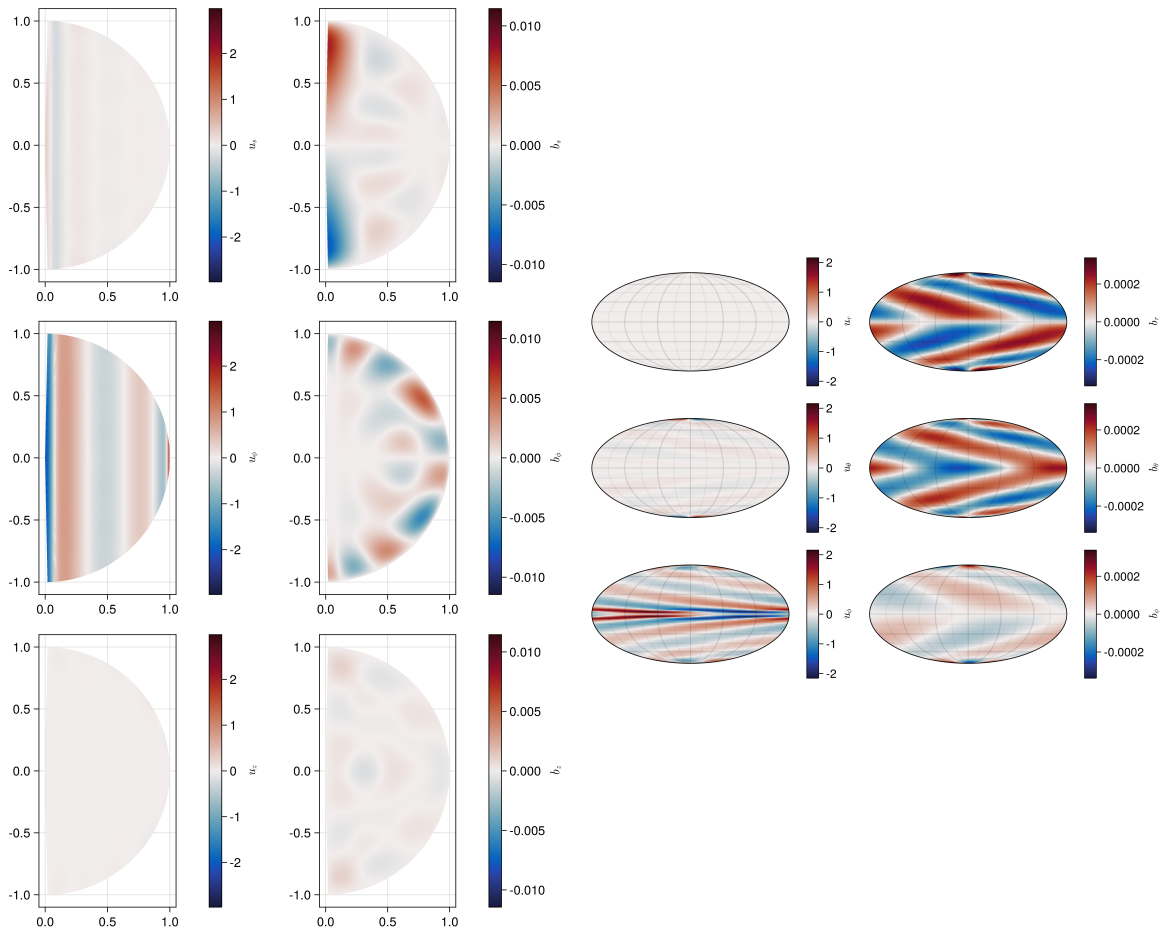


Figure A.1: Meridional section (left) and surface expression (right) of a 3-D QGMC mode

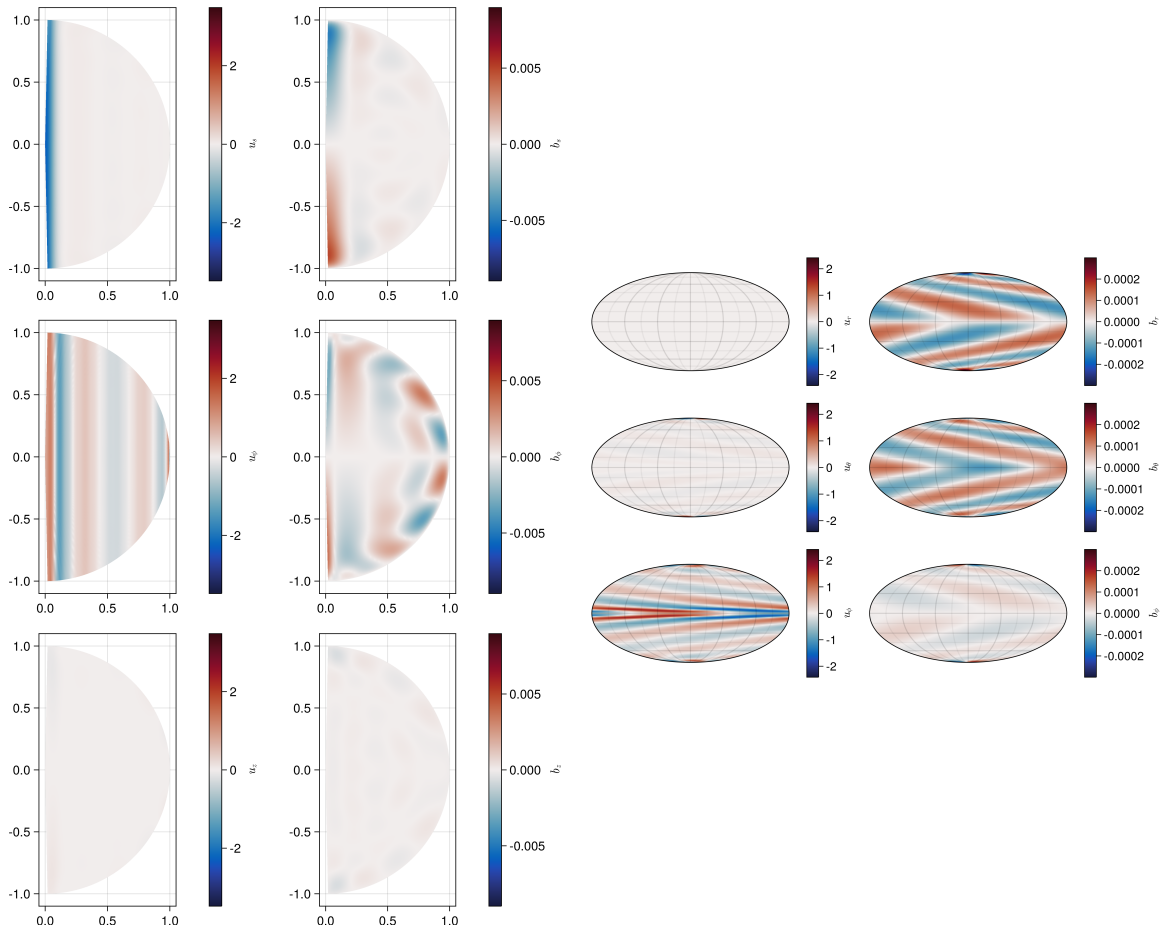


Figure A.2: Meridional section (left) and surface expression (right) of a 3-D QGMC mode

# Bibliography

- Holdenried-Chernoff, Daria (2021). “The long and short timescale dynamics of planetary magnetic fields”. en. Accepted: 2021-10-15T06:43:38Z. Doctoral Thesis. ETH Zurich. doi: [10.3929/ethz-b-000509840](https://doi.org/10.3929/ethz-b-000509840). URL: <https://www.research-collection.ethz.ch/handle/20.500.11850/509840> (visited on 07/26/2023).
- Jackson, Andrew and Stefano Maffei (Nov. 2020). “Plesio-geostrophy for Earth’s core: I. Basic equations, inertial modes and induction”. In: *Proceedings of the Royal Society A: Mathematical, Physical and Engineering Sciences* 476.2243. Publisher: Royal Society, p. 20200513. doi: [10.1098/rspa.2020.0513](https://doi.org/10.1098/rspa.2020.0513). URL: <https://royalsocietypublishing.org/doi/10.1098/rspa.2020.0513> (visited on 02/13/2023).